eNeuro

Research Article: New Research | Disorders of the Nervous System

Introduction of tau oligomers into cortical neurons alters action potential dynamics and disrupts synaptic transmission and plasticity

https://doi.org/10.1523/ENEURO.0166-19.2019

Cite as: eNeuro 2019; 10.1523/ENEURO.0166-19.2019

Received: 7 May 2019
Revised: 29 August 2019
Accepted: 12 September 2019

Manuscript Title

Introduction of tau oligomers into cortical neurons alters action potential dynamics and disrupts synaptic transmission and plasticity

Abbreviated Title

Oligomeric tau alters neuronal and synaptic properties

Author names and affiliations

Emily Hill[a*], Thomas K. Karikari[a], Kevin G. Moffat[a], Magnus JE Richardson[b] and Mark J Wall[a]

[a] School of Life Sciences, University of Warwick, Coventry, CV4 7AL

[b] Institute of Mathematics, University of Warwick, Coventry, CV4 7AL

Author Contributions

EH and TKK performed the experiments. EH, TKK and MJER analysed the data. MJW and EH planned the research and wrote the paper with comments from KGM, MJER and TKK.

Correspondence should be addressed to (include email address)

Mark wall (mark.wall@warwick.ac.uk) and Emily Hill (e.hill.2@warwick.ac.uk)

School of Life Sciences, University of Warwick, Gibbet Hill, CV4 7AL, UK

Abstract

Tau is a highly soluble microtubule-associated protein that acts within neurons to modify microtubule stability. However, abnormally phosphorylated tau dissociates from microtubules to form oligomers and fibrils which associate in the soma-dendritic compartment. Although tau can form neurofibrillary tangles (NFTs), it is the soluble oligomers that appear to be the toxic species. There is, however, relatively little quantitative information on the concentration- and time-dependent actions of soluble tau oligomers (oTau) on the electrophysiological and synaptic properties of neurons. Here, whole-cell patch clamp recording was used to introduce known concentrations of oligomeric full-length tau-441 into mouse hippocampal CA1 pyramidal and neocortical layer-V thick-tufted pyramidal cells. oTau increased input resistance, reduced action potential amplitude and slowed action potential rise and decay kinetics. oTau injected into presynaptic neurons induced the run-down of unitary EPSPs which was associated with increased short-term depression. In contrast, introduction of oTau into postsynaptic neurons had no effect on basal synaptic transmission, but markedly impaired the induction of long-term potentiation. Consistent with its effects on synaptic transmission and plasticity, oTau puncta could be observed in the soma, axon and in the distal dendrites of injected neurons.

Visual Abstract

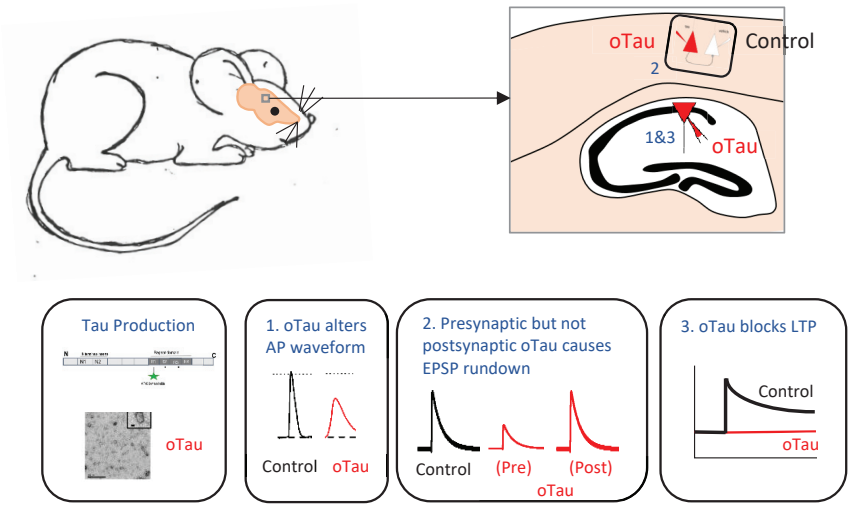

Significance statement

The protein tau is highly expressed in neurons and is involved in maintaining neuronal structure. In diseases such as Alzheimer's disease, tau can form oligomers, which consist of tau molecules joined together. There is growing evidence that these tau oligomers are toxic to neurons, although their precise actions are still being characterised. We have taken the approach of introducing structurally-defined tau-441 oligomers into neurons via the recording electrode (a method previously published by Kaufmann et al 2016). This method allowed us to provide detailed characterisation of the concentration- and time- dependent actions of tau oligomers on neuronal properties. We have found that tau interferes with the action potential waveform, modifies synaptic transmission and can block events that probably underlie memory storage.

Introduction

Tau is a native protein usually associated with microtubules and is key to maintaining cellular morphology, particularly in neuronal axons (Tracy and Gan 2018). Tau is also expressed in the dendrites and is involved in some forms of synaptic plasticity (Regan et al 2015). Under physiological conditions, the phosphorylation level of tau protein is regulated by the equilibrated action of kinases and phosphatases. However, dysfunctional states can induce hyperphosphorylation causing tau to disassociate from microtubules, altering their stability (Qiang et al., 2018), with the now free monomeric tau protein prone to aggregation (Avila et al., 2006). The hyperphosphorylated tau monomers initially polymerise to form soluble oligomers. These β-sheet-rich oligomers can then further aggregate into protofibrils, fibrils and neurofibrillary tangles (NFTs). Although NFTs are major histopathological hallmarks of neurodegenerative tauopathies (Nelson et al., 2009), there is strong evidence that the soluble oligomers are the toxic species and play a more important role in disease pathology. Previous studies have shown that tau overexpression leads to neuronal loss, synaptic and behavioural dysfunction without NFT accumulation (Lee et al., 2001; Tanemura et al., 2002; Tatebayashi et al., 2002; Wittmann et al., 2001; Andorfer et al., 2003; Spires et al., 2006; Yoshiyama et al., 2007; Cowan et al., 2010). Furthermore, the introduction of tau oligomers (oTau), either extracellularly or via injection into the brain of wildtype rodents induces synaptic, mitochondrial and memory dysfunction (Fá et al., 2016, Ondrejcak et al., 2018), consistent with the hypothesis that oTau are the drivers of toxicity. Alongside the direct effects of oTau, studies have also demonstrated its role in mediating the pathogenesis of other aggregating proteins including amyloid beta and alpha synuclein (Castillo-Carranza et al, 2015 and Teravskis et al, 2018 respectively).

Many previous electrophysiological investigations of the effect of oTau on neuronal properties have been carried out using extracellular application of oTau or transgenic

tauopathy mouse models, where mutant forms of tau protein, that are prone to aggregate, are overexpressed. In such studies, oligomeric tau has been shown to alter the intrinsic excitability of neurons and modulate short and long-term plasticity (Mondragón-Rodríguez et al., 2018; Tamagnini et al., 2017 and Rocher et al., 2010, Hoover et al., 2010). For example, Ondrejcak et al. (2018) suggested a postsynaptic action of oTau by showing that administrating intracerebroventricular injections, of either recombinant aggregated tau protein or tau protein isolated from human Alzheimer's disease (AD) patients, inhibited hippocampal long-term depression (LTP) with no effect on paired-pulse ratio. Dissociated tau protein (from viral expression) has also been shown to localise in presynaptic nerve terminals, binding to synaptic vesicles, reducing their mobilisation, fusion rate and rate of recycling (Zhou et al 2017).

In our study, *in vitro* electrophysiology (whole-cell patch clamp recording), together with detailed quantitative analyses has been used to fully characterise the effects of introducing tau oligomers (oTau) directly into cortical neurons. This approach has allowed the evaluation of the direct effects of oTau within a neural network that is free from tau pathology apart from the recorded neuron. Unlike previous studies, this has allowed the delineation of time- and concentration-dependent effects of oTau. Moreover, measuring the electrophysiological and synaptic properties of each neuron immediately after whole-cell breakthrough acts as an internal control for each recording. Using this approach, oTau can be introduced into either pre- or postsynaptic cells and the effects on synaptic transmission and plasticity measured. Such targeting is not possible in studies where oTau is applied via the extracellular solution as it is difficult to ascertain if the observed toxic effects are due to exogenous oTau affecting cell-membrane integrity or the direct intracellular effects of internalised oligomers. While the estimated physiological concentration of tau protein in neurons is 2 μM (Avila 2010), here we demonstrate that introduction of nanomolar concentrations of oTau into hippocampal or neocortical pyramidal neurons is sufficient to cause significant changes in action potential

kinetics, impair basal synaptic transmission and disrupt synaptic plasticity over a 45-50 minute time-frame.

Methods

Protein expression, purification and characterisation

Briefly, *Escherichia coli* BL21 (DE3) carrying pProEX plasmids (Promega) coding for wild-type full-length tau-441 (Uniprot ID: P10636-8) with N-terminal 6xHis and FLAG tags and cysteine modifications (C291A/C322A/I260C), were inoculated into Luria broth (15 ml) containing ampicillin (100 ug/ml) and chloramphenicol (35 µg/ml) and incubated at 37 °C at 180 rpm overnight. The purpose of the cysteine modifications was to have a single cysteine residue located outside the microtubule binding region that can be specifically labelled by a fluorophore without potentially interfering with the protein's functions; this approach has been widely used and shown to have no detrimental effects (Kumar et al., 2014, Michel et al., 2013, Shammas et al., 2015, Karikari et al., 2019). The starter cultures were added to 750 ml fresh LB broth with ampicillin (100 $\mu g\ ml^{-1}$) and returned to the shaking incubator for 90 minutes. When the OD600 reached 0.6, 0.5mM isopropyl β-D-1 thiogalactopyranoside was added for 1 hour. Samples were centrifuged for 10 mins at 4 °C at 9800g. The supernatant was removed, and pellets washed with 10 mM sodium phosphate pH 7.4 buffer twice. Pellets were re-dissolved in 10 mM sodium phosphate buffer pH 7.4 and stored at -20 °C until use. Samples were purified via immobilised metal affinity chromatography (IMAC).

Eluted fractions from IMAC were analysed using 6% non-denaturing sodium dodecyl sulfate polyacrylamide gel electrophoresis (SDS-PAGE) gels to determine the highest yields which were pooled and concentrated using Slide-A-LyzerTM MINI Dialysis devices (10K MWCO; Thermo Scientific). Briefly, the devices were washed with 1 ml sodium phosphate pH 7.4 buffer, the samples added and centrifuged for 30 mins at 2600xg at 4 °C. A bicinchoninic

acid assay (#786-570, G-Biosciences, Missouri, USA) was used to calculate the concentration and where needed the remaining liquid concentrated with further spins.

Preparation of fluorescently labelled oTau

Purified Tau-441 was treated with 5x molar excess of tris(2-carboxyethyl)phosphine (TCEP) for 1 h, and then with 4x molar excess of Alexa Fluor-maleimide (#A10254, Molecular Probes) overnight in the presence of sodium phosphate buffer pH 7.4. Free fluorophore and reducing agent were removed by 5 x 2 h repeat dialysis against 2 L of dialysis buffer (50 mM Tris HCl pH 7.5, 100 mM NaCl) in a Slide-A-LyzerTM MINI Dialysis device (10K MWCO) at each step. Non-denaturing SDS-PAGE followed by ultraviolet light exposure were used to confirm labelling, with efficiency spectrophotometrically estimated using Beer's law and molar extinction coefficient of tau-441. Unlabelled controls were prepared following the same protocol but with equal volume of 10 mM sodium phosphate buffer pH 7.4 instead of the maleimide label. The entire labelling process was performed at room temperature.

Circular dichroism (CD) spectroscopy

CD spectra were collected on unlabelled tau-441 diluted to 10 μM in sodium phosphate buffer pH 7.4. The sample was loaded in a 1-mm path-length cell and transferred to a Jasco J-815 CD spectropolarimeter Ten different spectra were taken on each sample and the average presented. The analytical conditions were: scan speed 100 nm/min, response time 1 s, data pitch 0.1 nm and high-tension voltage ≤550 V.

Transmission electron microscopy

Formvar/carbon-coated 300-mesh copper grids (#S162, Agar scientific, UK) were glow-discharged using the ELMO system from Cordouan Technologies. Five microliters of labelled or unlabelled tau-441 preparations were pipetted onto the grid and allowed to bind for 1 min. Excess samples were removed with a strip of filter paper, and 5 μl of 2 % uranyl

189 acetate added for 1 min. After removing the excess stain with a strip of filter paper, the grids
190 were imaged using a JEOL-2100F transmission electron microscope.
191
192 **Dynamic light scattering**
193 Size distributions of labelled proteins at 1 mg/ml were measured on a Zetasizer Nano ZS
194 machine (Malvern). Up to ten repeat measurements were obtained for each sample. The
195 'number distribution' function was used to compute the percentage size distribution of the
196 particles.
197
198 **Dot blot**
199 Two microliter aliquots of tau-441 (444 μM) dissolved in intracellular patching solution were
200 spotted onto nitrocellulose membranes, allowed to dry and then blocked with 10 % non-fat
201 milk in phosphate buffered saline (PBS) with 0.05 % Tween for 1 h. The membranes were
202 thereafter washed five times with 10 % Tris buffered saline (TBS)-Tween and incubated for 2
203 h with the primary antibodies diluted in PBS-Tween: T22 (#ABN454, Merck; 1000x dilution),
204 HT7 (#MN1000, ThermoFisher; 1000x dilution), K9JA (#A0024, Dako; 5000x dilution).
205 Subsequently, the membranes were re-washed five times with 10 % TBS-Tween and then
206 treated for 2 h with secondary antibody (anti-rabbit IgG #31450 or anti-mouse #62-6520,
207 Thermofisher). Following further washes, the membranes were developed with an
208 electrochemiluminiscent detection kit (BIORAD Clarity Western ECL #170-5060) and
209 imaged.
210
211 **Preparation of tau monomers**
212 oTau were incubated with 5 mM DTT (Sigma-Aldrich) for 30 mins at 60ºC to induce the
213 breakdown to monomers (Fa et al 2016). This conformational change was confirmed by non-
214 denaturing SDS-PAGE w 6% gels with protein bands detected after staining with Instant
215 Blue (Expedeon). All whole-cell patch experiments involving the introduction of monomeric
216 tau were completed within 3 h of the monomerisation protocol. To confirm that the tau

217 injected into neurons were monomeric, aliquots from the same monomerisation procedure
218 were mixed with the intracellular patch solution and resolved on SDS-PAGE gels as
219 described above.
220

221 ## Electrophysiology

222 **Preparation of hippocampal and neocortical brain slices**

223 All experiments were approved by the local Animals Welfare and Ethics Board (AWERB).
224 Male BL6 mice (~ 3-4 weeks and P12-21 for paired-synaptic transmission studies) were
225 killed by cervical dislocation and decapitated in accordance with the U.K. Animals (Scientific
226 Procedures) Act (1986). Parasagittal hippocampal and neocortical slices (350 μM) were cut
227 with a Microm HM 650V microslicer in cold (2-4°C) high Mg^{2+}, low Ca^{2+} aCSF, composed of
228 (mM): 127 NaCl, 1.9 KCl, 8 $MgCl_2$, 0.5 $CaCl_2$, 1.2 KH_2PO_4, 26 $NaHCO_3$, 10 D-glucose (pH
229 7.4 when bubbled with 95% O_2 and 5% CO_2, 300 mOSM). Neocortical slices were cut at an
230 angle of +15º, such that the blade started cutting from the surface (layer 1) of the neocortex
231 towards the caudal border of the neocortex (to ensure the integrity of layer V pyramidal cell
232 dendrites, Kerr et al 2013). Slices were stored at 34 °C in standard aCSF (1 mM Mg^{2+} and 2
233 mM Ca^{2+}) for between 1 to 8 hours.
234

235 **Whole-cell patch clamp recording from pyramidal cells**

236 A slice was transferred to the recording chamber, submerged and perfused (2-3 ml/min^{-1})
237 with aCSF at 30 °C. Slices were visualized using IR-DIC optics with an Olympus BX151W
238 microscope (Scientifica, Bedford UK) and a CCD camera (Hitachi). Whole-cell current-clamp
239 recordings were made from pyramidal cells in area CA1 of the hippocampus and from thick-
240 tufted layer-V pyramidal cells in the somatosensory cortex using patch pipettes (5–10 MΩ)
241 manufactured from thick walled glass (Harvard Apparatus, Edenbridge, UK). Pyramidal cells
242 were identified by their position in the slice, morphology (from fluorescence imaging) and
243 characteristics of the standard current-voltage relationship. Voltage recordings were made

using an Axon Multiclamp 700B amplifier (Molecular Devices, USA) and digitised at 20 KHz. Data acquisition and analysis were performed using pClamp 10 (Molecular Devices). Recordings from neurons that had a resting membrane potential of between -60 and – 75 mV at whole-cell breakthrough were accepted for analysis. The bridge balance was monitored throughout the experiments and any recordings where it changed by more than 20 % were discarded. Tau-protein oligomers, from a 22 μM stock (monomer concentration), were added to filtered intracellular solution containing (mM): potassium gluconate 135, NaCl 7, HEPES 10, EGTA 0.5, phosphocreatine 10, MgATP 2, NaGTP 0.3 (293 mOSM, pH 7.2) to give a final concentration of either 44 nM, 133 nM or 444 nM tau-protein oligomers for CA1 neurons (2, 6 and 20 μg/ml tau) and 666 nM for layer-V pyramidal cells (30 μg/ml tau). Intracellular solution was filtered before the addition of tau-protein oligomers.

Stimulation protocols

To extract the electrophysiological properties of recorded neurons, both step and more naturalistic, fluctuating currents were injected at 10-minute intervals for a duration of the recordings (as show before in Kaufmann et al 2016).

Standard IV protocol

The standard current-voltage relationship was constructed by injecting step currents from -200 pA (CA1 pyramidal cells) and -600 to -400 pA (layer V pyramidal cells) incrementing by either 50 or 100 pA until a regular firing pattern was induced (Figure 2). A plot of step current against voltage response around the resting potential was used to measure the input resistance (gradient of the fitted line).

Dynamic IV protocol

The dynamic-IV curve, defined by the average transmembrane current as a function of voltage during naturalistic activity can be used to efficiently parameterise neurons and

generate reduced neural models that accurately mimic the cellular response. The method has been previously described (Badel et al 2008; Harrison et al 2015 and Kaufman et al 2016); for the dynamic-IV computer code see Harrison et al (2015). Briefly, a current waveform, designed to provoke naturalistic fluctuating voltages, was constructed using the summed numerical output of two Ornstein–Uhlenbeck processes (Uhlenbeck & Ornstein, 1930) with time constants τ_{fast} = 3 ms and τ_{slow} = 10 ms. This current waveform, which mimics the stochastic actions of AMPA and GABA-receptor channel activation, is injected into cells and the resulting voltage recorded (a fluctuating, naturalistic trace). The voltage trace was used to measure the frequency of action potential firing and to construct a dynamic-IV curve. The firing rate was measured from voltage traces evoked by injecting a current waveform of the same gain for all recordings (firing rate ~2-3 Hz). Action potentials were detected by a manually set threshold and the interval between action potentials measured. Dynamic I-V curves were constructed and used to extract a number of parameters including the capacitance, time constant, input resistance, resting membrane potential, spike threshold and spike onset (Figure 2; Badel et 2008; Kaufmann 2016). Using these parameters in a refractory exponential integrate-and-fire (rEIF) model reliably mimics the experimental data, with a spike prediction of ~ 75-80 % as shown previously (Badel *et al*., 2008). All analyses of the dynamic-IV traces were completed using either Matlab or Julia software platforms (Bezanson et al., 2017).

Synaptic transmission

To measure synaptic transmission between connected neighbouring neocortical thick-tufted layer-V pyramidal cells, 2-3 simultaneous whole cell current-clamp recordings were made in somatosensory cortex (Markram et al 1997; Kerr et al 2013). Recordings were made from neurons in slices from P12-18 mice because unitary EPSPs have a larger amplitude than unitary EPSPs in slices from older mice and show marked short-term depression (Reyes and Sakmann 1999; Kerr et al 2013) which can be used to measure the effects of oTau on release probability. Once synaptic connectivity was detected, 6 action potentials were

evoked in the presynaptic neuron (5 at 20 Hz followed by a single recovery action potential after a 1 second interval) using 5 ms current steps. These stimulus trains were separated by 10 s and repeated for the duration of recordings. The amplitude of overlapping unitary EPSPs was accurately measured using voltage deconvolution and reconvolution (Richardson and Silberberg 2008; Kerr et al 2013).

To measure long-term potentiation (LTP), whole-cell current-clamp recordings were made from CA1 hippocampal pyramidal cells in the presence of 50 μM picrotoxin (to block $GABA_A$ receptors). Schaffer collaterals were stimulated with a concentric bipolar electrode (FHC, Maine USA) every 20 s and after a 15 minute baseline, LTP was induced by theta-burst stimulation (10 trains of 10 stimuli (100 Hz) separated by 100 ms). The stimulation strength was set to evoke reliable and robust synaptic transmission (EPSP amplitude ~ 3 mV) without producing action potential firing in the postsynaptic cell.

Statistical analysis

Analysis was performed using non-parametric Wilcoxon rank sum tests and ANOVA's in graphPad Prism (San Diego California USA). In the text, values are given as mean ± standard error of the mean. The mean ± standard deviation are given in table 1 and extended data table 1-1.

Immunohistochemistry – localisation of tau protein

Alexa Flour 594 Hydrazide dye (Molecular Probes) was added to the intracellular solution (0.05 mM final concentration) to allow cell visualisation. CA1 pyramidal neurons injected with labelled oTau were recorded for a minimum of 20 minutes to allow the diffusion of tau protein out of the pipette and into the cell. The pipette was then carefully removed from the cell, slices were fixed in paraformaldehyde (PFA, 4 %) overnight at 4 °C and washed 5 times for 5 minutes in PBS the next morning. Slices were mounted and fixed using Vectashield (Vector labs, Perterborough UK). A Leica 710 confocal microscope was used for imaging and Zen software for image processing. A subset of 4 neurons were fully reconstructed

using the Airyscan module (tiled Z-stacks consisting of ~28 stacks each of 260 z-planes) using the Leica 880 confocal microscope to investigate the distribution of oTau in the axon and dendrites.

Drugs

Picrotoxin (Sigma, Poole UK) and L689,560 (trans-2-Carboxy-5,7-dichloro-4-phenylaminocarbonylamino-1,2,3,4-tetrahydroquinoline, Hello-Bio, Bristol, UK) were made as stock solutions (1-50 mM) and diluted in aCSF on the day of use.

Results

Production and biochemical characterisation of human oTau

Recombinant full-length human tau-441, the longest tau isoform expressed in the human central nervous system (Figure 1a), was expressed in *E.coli*, labelled, oligomerised and characterised (as demonstrated in Karikari et al. 2017; Karikari et al. 2019). The tau preparation was labelled with Alexa Fluor-488 to block the formation of high molecular-weight aggregates and fibrils and to allow the tracking of oTau in recorded neurons. The expressed oTau had a spherical/granular structure, as shown by negative-stain electron microscopy (Figure 1B/C). CD spectroscopy showed a single negative peak at ~208 nm (Figure 1E), an intermediate between those peaks typical for monomers and filaments (200 nm and 220 nm respectively) suggesting the presence of beta-sheet structures (von Bergen et al., 2005, Karikari et al., 2017). The CD spectrum was similar when the cysteine residues were not mutated showing that this alteration had little effect on secondary structure (Figure 1E). Dynamic light scattering showed that monomeric Tau had a uniform small size (mean size = 8 ± 3.2 nm, with ~80% of the particles having a size between 7.5 – 10 nm). In contrast, oTau was larger and had a wider size distribution with ~93% particles measuring between 18-32 nm (Figure 1F). oTau that was diluted into intracellular recording solution reacted strongly with the T22 oligomer-preferring antibody (Figure 1d) thus the Tau protein

354 remains in an oligomeric form. The same oTau preparations also reacted strongly with HT7
355 and K9JA antibodies, which bind to the mid-region and microtubule binding region tau
356 respectively (Figure 1D).
357
358 **Effects of oligomeric tau on CA1 pyramidal cell subthreshold electrophysiological**
359 **properties**
360 Two controls were used in the electrophysiological recording experiments. First, a vehicle
361 solution (sodium phosphate pH 7.4 buffer), treated with the same labelling protocol as tau
362 protein, was added to the intracellular solution (at the same volume as the oTau). Second, to
363 ensure that the addition of a protein to the intracellular solution did not produce non-specific
364 effects, BSA (bovine serum albumin) was added to the intracellular solution (20 μM). BSA
365 has a similar molecular-weight to tau monomers and was injected at higher concentration
366 than oTau (20 μM vs 44-666 nM).
367
368 The two controls and oTau, each diluted in the intracellular solution, were introduced into
369 hippocampal CA1 pyramidal cells via the recording electrode during whole-cell current-
370 clamp recording. Following the termination of recordings (after ~50 minutes), slices were
371 fixed and the recorded cells visualised with confocal microscopy. The presence of oTau
372 could be observed in the somatic compartment of recorded neurons (Figure 2A). Standard
373 and dynamic IV protocols (Figure 2B, C) were used to extract electrophysiological
374 parameters from neurons where different concentrations of oTau (44, 133 and 444 nM),
375 vehicle or BSA had been introduced. Electrophysiological parameters were then compared
376 between the first time point (0-5 minutes after whole cell breakthrough) and at 40 minutes,
377 where the majority of recordings were still stable. At the initial time point, Kruskal-Wallis tests
378 confirmed that there were no significant differences in any of the electrophysiological
379 parameters (resting potential, input resistance, capacitance, time constant, spike threshold
380 and spike onset) from neurons injected with the different agents (n = 10 slices for vehicle, n

= 5 slices for BSA, *n* = 9 slices for oTau 44 nM, *n* =11 slices for oTau 133 nM and *n* =10 slices for oTau 444 nM, Table 1). Therefore, the initial quality of recordings and neural properties were comparable across all the experimental treatments. Most of the extracted parameters did not significantly change over the duration of recordings for cells that had either been injected with vehicle, BSA, 44 nM or 133 nM oTau (Figure 3A, B). However, there was a significant increase in input resistance (176.8 ± 4.73 mΩ to 239.3 ± 36.3 mΩ, p = 0.0020) and depolarisation of the resting potential (-67.98 ± 1.69 mV at 0 mins and -61.79 ± 1.655 mV, p=0.0494) measured after 40 minutes for neurons injected with 444 nM oTau (Figure 3C). Consistent with this increase in input resistance and membrane potential depolarisation, there was also a significant increase in the action potential firing rate in cells injected with 444 nM oTau (p=0.0254) and although not reaching overall significance, six out of seven cells injected with 133 nM oTau also had an increased firing rate.

oTau markedly slows action potential dynamics and reduces action potential amplitude

The dynamic IV parameter extraction was effective for all conditions at 0 mins (mean spike match of 72.2 ± 1.7 %, predicted vs experimental data). However, for the cells with oTau introduced, by 40 mins the model predictions were unable to accurately match the experimental spike data (mean spike match of 46.1 ± 5.5 %) and therefore wasn't used to extract parameters at later time points. To establish why there might have been a drop in spike match efficiency, we looked at whether there were changes to the parameters that define the action potential waveform (amplitude, duration, rate of rise and decay). There was no significant difference in any of these parameters at time zero across all of the experimental treatments using Kruskal-Wallis tests (Table 1). However significant changes in the action potential waveform were observed at the 40-minute time-point for all of the concentrations of oTau (Figure 4A, B) but were not observed when neurons were injected with either vehicle or BSA (Figure 4A, B). For all three concentrations of oTau (44, 133, and 444 nM), there was a significant decrease in action potential amplitude, speed of rise and

409 speed of decay at 40 minutes compared to time zero (Fig 4B). The time-course for these
410 changes in action potential parameters (amplitude and rate of rise) were examined for the
411 different concentrations of oTau (Figure 4C, D). The effects of 444 nM oTau occurred
412 significantly earlier than for 44 and 133 nM oTau (10 vs 20 minutes), characteristic of
413 concentration-dependent effects.
414
415 **The changes in action potential amplitude and kinetics do not occur with monomeric**
416 **tau protein**
417 Given a previous report that some populations of monomeric tau can readily seed
418 aggregation to form toxic oligomers (Mirbaha et al., 2017), we decided to investigate
419 whether tau protein monomers can induce changes in the action potential waveform or
420 whether only oTau is responsible. Tau monomers (mTau) (444 nM, see methods, Figure 5A)
421 were injected into hippocampal pyramidal cells. There was no significant change in the
422 current-voltage relationship over-time for neurons injected with mTau (Figure 5B) and no
423 change in action potential amplitude (at 40 mins the mean amplitude was 98.6% of the
424 amplitude at time 0, Figure 5C). It is therefore only the oligomeric form of tau that induces
425 the changes in neuronal electrophysiological properties over a time-scale of ~ 40 minutes.
426 However, it is possible that at longer time scales the monomeric tau may oligomerise and
427 then start to have effects on neuronal properties.
428
429 **The changes in action potential waveform cannot be accounted for by the**
430 **aggregation of oTau increasing series resistance.**
431 The reduction in action potential amplitude and the slowing of rise and decay kinetics could
432 be a result of electrotonic filtering due to an accumulation of oTau aggregates in the tip of
433 the patch pipette increasing series resistance. This seems unlikely as there was no
434 significant difference in series resistance between recordings made with vehicle in the patch
435 pipette and with oTau (Figure 5D). There was also no marked change in series resistance
436 over the length of recordings when either oTau or vehicle were introduced into cells (Figure

5D). To provide further confirmation, we carried out re-patching experiments (as in Fang et al., 2014 Fig 5E-J). Following whole-cell recording from a pyramidal cell for 20 minutes with either oTau (444 nm) or vehicle (control), the electrode was carefully removed from the cell surface and the cell was then re-recorded with an electrode which contained intracellular solution with vehicle (Fig 5E, J). The changes in action potential kinetics induced by oTau were still present when cells were re-patched with pipettes containing intracellular with vehicle (Fig 5 I, J). The re-patching of cells which had originally been recorded with vehicle containing intracellular solution had no effect on action potential kinetics or amplitude (Fig 5F, G). Therefore the changes in action potential dynamics were not the result of oTau accumulating in the patch pipette or at the site of whole-cell breakthrough.

Introduction of oTau into presynaptic cells markedly impairs basal synaptic transmission.

Given the marked of effects of oTau on action potential kinetics, the next step was to investigate if oTau introduction affected synaptic transmission. Due to the low connectivity between hippocampal pyramidal cells - between 1 and 5% (Debanne *et al.,* 2008), the synapses between pairs of thick-tufted layer-V neocortical pyramidal cells (layer V PCs) were examined instead. Initially we confirmed that the introduction of oTau (444 nM) into layer V PCs had similar effects on action potential properties to that observed in hippocampal CA1 pyramidal cells. Action potential amplitude was significantly reduced from 74.45 ± 2.13 mV at time zero to 60.135 ± 6.38 mV after 40 minutes ($p = 0.0137$) in cells where oTau was injected ($n = 8$, Figure 6A). There was no significant change in the amplitude of action potentials in neurons injected with vehicle (mean of 80.85 mV ± 1.82 at 0 mins vs 77.87 mV ± 2.08 at 40 mins, $p = 0.1337$, $n = 10$). Injection of oTau also significantly increased the input resistance (from 92.5 MΩ ± 7.58 at time zero to 108.19 ± 8.107 MΩ at 40 minutes $p = 0.0446$, Figure 6A) with no difference following the introduction of vehicle (90.1 ± 11.95 MΩ vs. 92.15 ± 12.99 MΩ, $p = 0.672$). Because the effects of oTau were slower in

layer-V thick-tufted pyramidal cells, presumably due to their larger size, we used a larger concentration of tau (666 nM) so that any changes in the properties of synaptic transmission occurred within a manageable time frame. To test whether oTau affected synaptic transmission, oligomer preparations were introduced into the presynaptic cell and vehicle was introduced into the postsynaptic cell (Fig 6C). A train of five APs followed by a recovery AP (1 s interval, Kerr et al Figure 5D) was used to test whether layer-V pyramidal cells were synaptically connected. Once the connectivity was verified, this stimulus was repeated (at an interval of 10 s) through-out the duration of recordings (up to ~ 50-60 minutes). For the first EPSP, the amplitude and latency were measured from average EPSPs (Fig 6E). Because of the small amplitude of unitary EPSPs (average amplitude ~ 0.6 mV), average EPSPs (between 30 and 50 sweeps) were evaluated over the following time periods: 0-10 minutes, 10-20 minutes, 20-30 minutes and 30-40 minutes. Deconvolution and then reconvolution enabled the accurate measurement of the amplitude of individual average EPSPs in the train in most recordings (Fig 6F). However, in a small number of recordings the amplitude of the EPSPs in the train were so small that they could not be accurately resolved and thus these connections were only used for analysis of the first EPSP.

Out of 230 paired recordings, 25 pairs of neurons were synaptically connected (1 in 9.2 pairs). In 10 of the connected pairs, vehicle was introduced into both the pre and postsynaptic cells (as a control). In another 10 connections, oTau was introduced into the presynaptic cell and vehicle was introduced into the postsynaptic cell and in a further 4 recordings, oTau was introduced into the postsynaptic cell and vehicle in the presynaptic cell. At early time points (0-10 minutes) there was no significant difference in the amplitude of the first EPSP in the train ($p = 0.51$) or its latency ($p = 0.581$) when either vehicle or oTau were introduced into the presynaptic cell (mean unitary EPSP amplitude: vehicle 0.75 ± 0.13 mV; oTau 0.61 ± 0.13 mV; latency: vehicle 2.2 ± 0.0002 ms, oTau 2.1 ± 0.0001 ms). When vehicle was introduced into both the pre and postsynaptic cells, the amplitude of the first EPSP in the train remained relatively stable for the duration of recordings (the amplitude of

the first EPSP after 40-50 minutes of recording was 90.5 ± 14 % of the EPSP amplitude at 0-10 minutes of recording). However, when oTau was introduced into the presynaptic cell, although the recordings remained stable (mean membrane potential at time zero -67.5 ± 1.5 mV vs membrane potential 40 minutes -62.5 ± 1.3 mV), the amplitude of the first EPSP in the train was markedly diminished in 7 out of 9 of the recordings. At 40-50 minutes, the amplitude of the first EPSP was significantly ($p = 0.034$) reduced to 30 ± 10 % of the amplitude of EPSPs at 0-10 minutes ($n = 9$, Figure 7A, B). This reduction in EPSP amplitude was not a result of failed action potential firing in the presynaptic cell, as the small number of sweeps in which any of the action potentials in the train failed (46 out of 3900 sweeps, ~ 1.2 %) were excluded from analysis. This indicates that the introduction of oTau into the presynaptic cell leads to a marked impairment in synaptic transmission between layer-V pyramidal neurons that occurs within a short time frame.

The deficits in synaptic transmission are associated with increased short-term depression

We next examined whether short term synaptic plasticity was altered by oTau by measuring the degree of depression induced by firing 5 action potentials at 20 Hz (50 ms interval). If the reduction in EPSP amplitude induced by oTau is a consequence of a fall in the probability of transmitter release, then short-term depression may be reduced (equivalent to the activation of presynaptic receptors such as adenosine A_1, for example see Kerr et al 2013). For analysis, the amplitude of EPSPs in the train (2^{nd}-5^{th}EPSP) were measured relative to the amplitude of the first EPSP. In 9 out of 10 recordings (in one recording the connection was too weak to accurately measure the amplitude of the 2^{nd} -5^{th} EPSPs) with vehicle introduced into both the pre and postsynaptic cells, there was little change in the degree of short-term depression over the duration of the recordings (Figure 7C, D). There was a small (but significant) increase in depression as there was a decrease in the paired-pulse ratio (second EPSP/first EPSP amplitude) over 40 minutes (Figure 7G). In the recordings (8 out of 9, one connection was too weak to accurately measure) where oTau was introduced into the

presynaptic cell there was an increase in the degree of short-term depression (Figure 7E, F). In 4 out of the 8 connections there was a failure of transmission: the 2^{nd}-5^{th} EPSPs were absent (Figure 7E). This was not a result of failed action potential firing, as any failures of presynaptic firing were excluded from analysis (as outlined above). There was also a significant decrease in the paired-pulse ratio (first EPSP/second EPSP) but this was comparable to the connections with vehicle in pre and postsynaptic cells. To examine the duration of the depression, we measured the relative amplitude of the recovery EPSP, which was evoked 1 s after the train of action potentials (Figure 7H). Even though there was greater depression in connections with oTau present in the presynaptic cell, the recovery (amplitude of recovery EPSP/first EPSP amplitude) was not different to connections with vehicle introduced into pre and postsynaptic cells. This indicates that the additional short-term depression induced by oTau recovers over the same period as the depression in control conditions. Therefore, the impairment of synaptic transmission is associated with an increase in depression and thus differs from the activation of presynaptic receptors.

Introducing oTau into the postsynaptic cell does not impair basal synaptic transmission

In four connected pairs of layer-V pyramidal cells, oTau was introduced into the postsynaptic cell with vehicle introduced into the presynaptic cell (Figure 8A). In these connections, there was no significant reduction in the amplitude of the first EPSP in the train over time (average EPSP amplitude after 40 minutes was 91.8 % of the EPSP recorded at 0-10 minutes, Figure 8B, C) and there was little change in short-term depression over-time (Fig 8D, E). Unlike the marked effects observed when oTau was introduced into the presynaptic cell, introduction of oTau into the postsynaptic neuron did not impair basal synaptic transmission over the duration of the recordings.

Postsynaptic oTau injection impairs long-term potentiation

Although introduction of oTau into the postsynaptic neuron had no effect on basal synaptic transmission it may modulate synaptic plasticity, as it has been suggested that the inhibitory effects of extracellular oTau on long term potentiation (LTP) are postsynaptic (Ondrejcak et al. 2018). To investigate this possibility, we made whole-cell current-clamp recordings from CA1 hippocampal neurons and stimulated Schaffer collaterals (Figure 9A). We took this approach as access to presynaptic neurons was not required and it is much more straightforward to carry out the experiment in hippocampal slices. oTau, vehicle or mTau were introduced into the postsynaptic neuron during current-clamp recording and the effects on long-term potentiation (LTP) measured. There was no significant difference in the amplitude of EPSPs across all of the conditions at time zero (One-way ANOVA, p=0.14783). When vehicle was introduced into the postsynaptic cell, theta-burst stimulation (TBS) induced robust potentiation (30 minutes after the stimulation, EPSP amplitude was 3.31 ± 1.32x the baseline amplitude, *n* = 7, Fig 9B, F). This potentiation was NMDA receptor-dependent as it was abolished by the NMDA receptor antagonist L689,560 (5 μM, 0.53 ± 0.14x the baseline EPSP amplitude after 30 minutes, *n* = 3, Fig 9B, F). In initial experiments we found that oTau (444 nM) abolished both STP and LTP (*n* = 7 slices, Fig 9C, F). The experiments were repeated with a 10 fold reduction in the concentration of oTau (44 nM) which also abolished LTP but did not prevent STP (n = 5, Figure 9D, F). Monomeric tau (444 nM) had little effect on the degree of potentiation (LTP or STP, *n* = 5, Fig 9E, F). This indicates that, the presence of oTau in postsynaptic cells will interfere with synaptic plasticity which could relate to early changes in learning behaviour. One possible mechanism for this interference with plasticity is a change in the voltage response to the theta-burst stimulation leading to a subthreshold depolarisation. To investigate this possibility, we examined the TBS voltage responses and found that there was large variability in response to TBS within control recordings (vehicle in the postsynaptic cell). There were some responses where the postsynaptic cell did not fire, where the cell fired repeatedly across all the bursts and where the cell only fired in response to the first burst. However robust LTP was produced in all cases. We observed a similar range of responses across all of the conditions, with no

correlation between LTP size and firing pattern (Figure 9G). Therefore it appears unlikely that a reduction in stimulus-response can account for the loss of LTP and also because the oTau is only in the postsynaptic cell it can be accounted for by impairment of basal synaptic transmission.

The effects of oTau on synaptic transmission and LTP strongly suggest that oTau must reach synaptic locations. To investigate this, we fully reconstructed a subset of four hippocampal neurons in which 444 nM oTau was introduced into the soma via a patch pipette and recordings were made for 20 minutes. In these neurons, puncta of oTau could clearly be observed in the distal dendrites (upto the bifurcation) and could also be observed in the axon (Figure 9H). This indicates that the introduced oTau can spread from the soma into dendritic and axonal compartments in ~ 20 minutes and is consistent with the effects on neurophysiology.

Discussion

This is the first study to investigate the effects of introducing oligomeric tau protein (oTau) directly into the soma of mammalian neurons in acute brain slices and then using whole-cell patch clamp recording to investigate the resultant changes in electrophysiological properties and synaptic transmission.

In several previous studies, tau oligomers have been applied to brain slices and neuronal cultures via the extracellular media (Lasagna-Reeves et al., 2012, Fá et al., 2016, Puzzo et al., 2017, Booth et al., 2016). Although tau has clear effects in these studies, it is difficult to determine if tau is acting on the outside of neurons, to quantify how much tau is taken up into neurons and whether the observed effects on synaptic transmission are pre or postsynaptic. Transgenic models of tauopathies have also been used to investigate changes in neuronal properties produced by tau (Zhou et al 2017; McInness et al 2018, Rudinskiy et al., 2014). In these studies, it is difficult to measure the concentration of oTau present and the specific oTau conformers that mediate the toxicity. The successful use of

patch clamp electrodes to introduce characterised alpha-synuclein oligomers into mammalian neurons has been published previously (Kaufmann et al., 2016). Here, utilising the same strategy, we have measured the time- and concentration-dependent effects of oTau. A major difference between our study and previous studies (apart from the method of introducing tau oligomers) is that only one neuron in a network will be affected by the introduced tau. This means that any changes in electrophysiological properties that are measured are direct and do not arise from compensatory changes in networks that may occur if the properties of many neurons are affected. Other major advantages of our approach include using the neuron (at whole-cell breakthrough) as an internal control for each recording and the removal of any slow cellular uptake steps which maybe present when tau is applied extracellularly. Furthermore, this method only requires a small amount of oTau and allows the targeting of oTau into either pre or postsynaptic neurons.

We utilised a method to prepare oTau which did not involve any inducers (such as heparin, RNA etc) as they may potentially produce cellular effects themselves. We have used AF-488 to label and also to limit the aggregation to oTau into fibrils. While an obvious caveat to this method is that we have mutationally altered tau-441, CD spectral analysis shows the mutations and labelling have only minor effects on tau structure (Figure 1E). More importantly, we have now established a proof of principle in the successful performance of these studies that in the future can be extended for in-depth analysis of different oTau preparations including tau with clinically relevant mutations. The oTau we prepared had a granular/spherical structure and a predominant β-sheet conformation (Fig. 1). The oTau reacted strongly to the T22 oligomeric tau antibody, the HT7 mid-region tau antibody and the K9JA tau repeat domain-binding antibody. We have confirmed that the tau preparations used for electrophysiological analysis were oligomeric, bearing the aggregation-defining repeat domain and a clinically relevant mid-region epitope used in biomarker tests for tauopathies (Chen et al., 2019). The tau oligomers were diluted into the intracellular solution after filtering to prevent binding to the filter and loss of protein (figure 1). Clearly the tau

631 could oligomerise in vitro, although it was not in a hyperphosphorylated state. In contrast
632 hyperphosphorylation has been implicated in the oligomerisation process that occurs in vivo
633 (Qiang et al., 2018; Avila et al., 2006). Taken together this suggests that the
634 hyperphosphorylation may be required for the dissociation of tau from the microtubules in
635 vivo but not for the oligomerisation step.
636
637 One interesting question is what is the phosphorylation state of the tau oligomers once they
638 have been introduced into the neurons? Since the oligomers were un-phosphorylated before
639 their introduction into neurons, any changes in the phosphorylation status post introduction
640 (whether to the introduced oligomers or endogenous tau) might play a role in the mechanism
641 of the observed effects. Experiments on phospho-tau status are often reported using
642 Western blots and densitometry. However, this is not a feasible way to determine tau
643 phospho-status, using our single cell introduction method. More recently new mass
644 spectrometric assays have been developed, Barthélemy et al (2019), but again require
645 substantial material to determine changes in phospho-status. Furthermore, the full length
646 oligomers used in this study contain around 80+ epitopes that can be phosphorylated. While
647 specific phospho-Ser/Thr/Tyr antibodies are available for several of these, it is unlikely that a
648 single cell immunofluorescence analysis will yield interpretable results.
649
650 **The effects of tau oligomers are not due to accumulation of aggregates in pipette or in**
651 **area of whole-cell break-through**
652 A number of control experiments were used to validate that the effects of oTau introduction
653 were specific and not an artefact of the recording and introduction protocol. There was no
654 significant difference in the electrophysiological parameters following the introduction of
655 vehicle (buffer without tau) or the addition of a similar size aggregation-competent molecule,
656 bovine serum albumin (BSA 20 μM). It is conceivable that either the narrow tip of the patch-
657 pipette becomes clogged with aggregated tau or tau accumulates in the soma around the
658 breakthrough site leading to filtering of the signals (particularly the action potential). Three

pieces of experimental evidence makes this seem unlikely. Firstly, there was no difference in either the initial series resistance across the conditions and no significant increase in series resistance for the duration of the recordings (see Figure 5D). Secondly, in re-patching experiments the changes in action potential amplitude and kinetics persisted when the cells were re-patched with intracellular solution containing vehicle. Finally, when oTau was introduced into the postsynaptic cell it had no effect on the amplitude or kinetics of the recorded EPSPs. If the effects of oTau were simply a filtering effect, then the EPSP amplitude would be expected to decrease and EPSPs would also have slower rise and decay kinetics. It has been shown before that alpha-synuclein oligomers (at a similar concentration, 500 nM) which were injected into cortical neurons, had no effect on action potential amplitude and the action potential rise and decay kinetics were not slowed (Kaufmann et al 2016). This suggests that the introduction of aggregating oligomeric species does not produce generalised filtering effects per se.

Tau oligomers modify action potential amplitude and kinetics but have little effect on subthreshold properties

Using standard step and dynamic current-voltage responses, we found that oTau had little effect on the majority of the subthreshold parameters that were measured. It was only at late time points (after 40 minutes) and with the larger concentrations of oTau (444-666 nM) that significant changes in input resistance (increased) and membrane potential (depolarised) occurred leading to an increased action potential firing rate. It may be that lower concentrations of oTau (44-133 nM) would eventually have effects on input resistance and membrane potential if the recordings lasted long enough (a small increase in firing rate was observed at late time points for 6 out of 7 cells with 133 nM oTau). An increase in input resistance could result from the block of a standing (or leakage) conductance or possibly from the electronic conversion of the cell from multi compartments to a single compartment by reducing current flow. The oTau-induced depolarisation is consistent with previously reported data from the rTg4510 mouse model, which expresses human tau variant P301L,

where the pyramidal cells are depolarised by ~ 8 mV compared to WT littermates (Rocher et al 2010).

oTau markedly altered the action potential waveform causing a slowing of rise and decay kinetics and a reduction in peak amplitude. These effects were concentration-dependent, occurring more rapidly with larger concentrations of oTau and did not occur with tau monomers. The mechanism underlying these changes in action potential waveform are currently not clear. It is possible that the aggregation of oTau in the soma act as a barrier to current flow from the initial segment in the axon (where Na+ channels are concentrated) to where the action potential is recorded in the soma or it could be due to changes in voltage gated Na^+ or K^+ channels.

Presynaptic tau oligomer injection impairs synaptic transmission

The introduction of oTau into the presynaptic neuron led to a large reduction in synaptic strength, an effect which was not observed when oTau was introduced into the postsynaptic neuron or if vehicle was introduced into both pre and postsynaptic neurons. An inhibition of synaptic transmission has been previously reported in transgenic tau models (Zhou et al 2017; McInes et al 2018). The inhibition of transmitter release by the activation of presynaptic receptors (such as adenosine A_1 or $GABA_B$) is associated with an increase in paired-pulse ratio and a reduction in depression across a train of EPSPs (Kerr et al 2013). This contrasts with the inhibitory effects of oTau which were not associated with a decrease in depression across a train of stimuli. In many of the recordings, the later EPSPs in the train failed, although there was some recovery of transmission following a 1 s interval. It has been reported in synapses between cultured hippocampal neurons from transgenic mice expressing tau that synaptic depression is enhanced and that this results from the crosslinking of vesicles with actin to slow vesicle movement (Zhou et al 2017). Our data is consistent with a reduction in the rate of vesicle restock although this does not account for the change in the first EPSP.

Does the change in action potential waveform contribute to the inhibition of synaptic transmission? Injection of human tau into the squid axon has been shown to result in inhibition of synaptic transmission without changing the action potential waveform (Moreno et al 2016) suggesting that tau can directly affect the release machinery in the synaptic terminal. It is possible that the changed dynamics of the action potential waveform interferes with propagation down the axon to the release sites, leading for example, to branch-point failure. This however seems unlikely, as it has been previously shown that complex spikes consisting of 2-3 full sized action potentials followed by several highly attenuated "spikelets" are all fully propagated down the axon of CA1 pyramidal cells (Apostolides et al 2016).

Postsynaptic oTau disrupts long term potentiation

Introduction of either 44 or 444 nM oTau into postsynaptic hippocampal neurons prevented the induction of long-term potentiation (LTP), with 444 nM also abolishing short term potentiation. These effects were not observed when either vehicle or monomer (444 nM) was introduced into postsynaptic neurons. Previous studies have shown that extracellular oTau can induce impair LTP (Fá et al 2016, Lasagna-Reeves et al, 2012) with monomeric tau inactive. In these experiments, oTau was introduced via the extracellular medium and thus it is unclear whether the site of action was either pre- or postsynaptic or there was activity at both sites. Ondrejack et al (2018) demonstrated that for a subset of AD brain extracts, that produced amyloid beta-independent reductions in LTP, immunodepletion of the extract with the Tau5 monoclonal antibody prevented the impairment of LTP. These studies provide a strong argument for testing the effect of direct neuronal oTau introduction on LTP. Our study validates the results of previous studies and also provides direct evidence that the postsynaptic effects of oTau are sufficient to abolish LTP. The observed defects in LTP could result from oTau increasing the threshold for LTP induction or by blocking LTP induction mechanisms. The former could be the result of oTau changing the voltage response to the TBS so that insufficient depolarisation reaches the dendritic spines to remove the NMDA receptor Mg^{2+} block. Although this possibility cannot be completely ruled

742 out, it appears unlikely as there were no consistent changes in TBS voltage responses and
743 the responses were highly variable under control conditions. Recent experiments have
744 highlighted the importance of tau in plasticity (Regan et al 2015) with its correct
745 phosphorylation required for long term depression. It is possible that the introduced oTau
746 could bind or sequester the tau present in the dendrites leading to inhibition of plasticity.
747
748 Following whole-cell recordings (up to 40-50 minutes duration), fluorescent oTau could be
749 clearly observed in both the cell body of CA1 hippocampal pyramidal cells and also in the
750 distal dendrites and axons. This is consistent with the observed effects of oTAU on synaptic
751 transmission and plasticity.
752
753 **Concluding statement**
754 Using a targeted approach, we have introduced oTau into cortical neurons and have shown
755 rapid changes in electrophysiological properties, synaptic transmission and synaptic
756 plasticity.
757 **Acknowledgements**:
758 This work was primarily supported by the BBSRC funded doctoral fellowship held by EH.
759 Part of this work was also funded by the Alzheimer's Research Trust. TKK is now working at
760 the Department of Psychiatry and Neurochemistry, Institute of Neuroscience and
761 Physiology, University of Gothenburg, Sweden, S34180. We thank Professor Nicholas Dale
762 for providing comments on the manuscript. We would also like to thank Ian Hands-Portman
763 for his assistance with the Zeiss Airyscan imaging and processing.
764
765 **Conflicts of Interest**
766 The authors declare no competing interests
767
768 **Funding sources**

EH holds a BBSRC funded doctoral fellowship. Part of this work was funded by the Alzheimer's Research Trust.

References

Andorfer, C., Kress, Y., Espinoza, M., De Silva, R., Tucker, K., Barde, Y., Duff, K. and Davies, P. (2003). Hyperphosphorylation and aggregation of tau in mice expressing normal human tau isoforms. Journal of Neurochemistry, 86(3), pp.582-590.

Apostolides, P., Milstein, A., Grienberger, C., Bittner, K. and Magee, J. (2016). Axonal Filtering Allows Reliable Output during Dendritic Plateau-Driven Complex Spiking in CA1 Neurons. *Neuron*, 89(4), pp.770-783.

Avila, J. (2010). Intracellular and extracellular tau. Frontiers in Neuroscience, 4.

Avila J, Santa-Marıa I, Perez M, Hernandez F, Moreno F. (2006) Tau phosphorylation, aggregation, and cell toxicity. J Biomed Biotechnol. 2006:74539.

Badel L., Lefort S., Brette., Petersen C.C.H., Gerstner W., Richardson M.J.E., 2008. Dynamic I-V Curves Are Reliable Predictors of Naturalistic Pyramidal-Neuron Voltage Traces. Journal of Neurophysiology, 99, 656-666.

Barthélemy NR et al (2019) Tau Phosphorylation Rates Measured by Mass Spectrometry Differ in the Intracellular Brain vs. Extracellular Cerebrospinal Fluid Compartments and Are Differentially Affected by Alzheimer's Disease. Front Aging Neurosci.

Bezanson, J., Edelman, A., Karpinski, S. and Shah, V. (2017). Julia: A Fresh Approach to Numerical Computing. SIAM Review, 59(1), pp.65-98.

795 Booth, C., Witton, J., Nowacki, J., Tsaneva-Atanasova, K., Jones, M., Randall, A. and
796 Brown, J. (2016). Altered Intrinsic Pyramidal Neuron Properties and Pathway-Specific
797 Synaptic Dysfunction Underlie Aberrant Hippocampal Network Function in a Mouse
798 Model of Tauopathy. Journal of Neuroscience, 36(2), pp.350-363.
799 Castillo-Carranza, D., Guerrero-Munoz, M., Sengupta, U., Hernandez, C., Barrett, A.,
800 Dineley, K. and Kayed, R. (2015). Tau Immunotherapy Modulates Both Pathological Tau
801 and Upstream Amyloid Pathology in an Alzheimer's Disease Mouse Model. Journal of
802 Neuroscience, 35(12), pp.4857-4868.
803 Chen, Z., Mengel, D., Keshavan, A., Rissman, R., Billinton, A., Perkinton, M., Percival-
804 Alwyn, J., Schultz, A., Properzi, M., Johnson, K., Selkoe, D., Sperling, R., Patel, P.,
805 Zetterberg, H., Galasko, D., Schott, J. and Walsh, D. (2019). Learnings about the
806 complexity of extracellular tau aid development of a blood-based screen for Alzheimer's
807 disease. *Alzheimer's & Dementia*, 15(3), pp.487-496.
808 Cowan, C., Chee, F., Shepherd, D. and Mudher, A. (2010). Disruption of neuronal
809 function by soluble hyperphosphorylated tau in aDrosophilamodel of tauopathy.
810 Biochemical Society Transactions, 38(2), pp.564-570.
811 Debanne, D., Boudkkazi, S., Campanac, E., Cudmore, R., Giraud, P., Fronzaroli-
812 Molinieres, L., Carlier, E. and Caillard, O. (2008). Paired-recordings from synaptically
813 coupled cortical and hippocampal neurons in acute and cultured brain slices. Nature
814 Protocols, 3(10), pp.1559-1568.
815 Fá, M., Puzzo, D., Piacentini, R., Staniszewski, A., Zhang, H., Baltrons, M., Li Puma, D.,
816 Chatterjee, I., Li, J., Saeed, F., Berman, H., Ripoli, C., Gulisano, W., Gonzalez, J., Tian,
817 H., Costa, J., Lopez, P., Davidowitz, E., Yu, W., Haroutunian, V., Brown, L., Palmeri, A.,
818 Sigurdsson, E., Duff, K., Teich, A., Honig, L., Sierks, M., Moe, J., D'Adamio, L., Grassi,
819 C., Kanaan, N., Fraser, P. and Arancio, O. (2016). Extracellular Tau Oligomers Produce
820 An Immediate Impairment of LTP and Memory. Scientific Reports, 6(1).

821 Fang, Q., Hu, W., Yang, Z., (2014). Enhancement of GABA-activated currents by
822 arginine vasopressin in rat dorsal root ganglions. Acta Physiologica Sinica, 66(6): 647-
823 657
824 Harrison PM, Badel L, Wall MJ & Richardson MJE (2015). Experimentally verified
825 parameter sets for modelling heterogeneous neocortical pyramidal cell populations.
826 PLoS Comput Biol 11, e1004165.
827 Hoover, B., Reed, M., Su, J., Penrod, R., Kotilinek, L., Grant, M., Pitstick, R., Carlson,
828 G., Lanier, L., Yuan, L., Ashe, K. and Liao, D. (2010). Tau Mislocalization to Dendritic
829 Spines Mediates Synaptic Dysfunction Independently of Neurodegeneration. *Neuron*,
830 68(6), pp.1067-1081.
831 Karikari, T.K., Nagel, D.A., Grainger, A., Clarke-Bland, C., Hill, E.J., Moffat, K.G., (2019).
832 Preparation of stable tau oligomers for cellular and biochemical studies. Analytical
833 Biochemistry 566, 67–74.
834 Karikari, T., Turner, A., Stass, R., Lee, L., Wilson, B., Nagel, D., Hill, E. and Moffat, K.
835 (2017). Expression and purification of tau protein and its frontotemporal dementia
836 variants using a cleavable histidine tag. Protein Expression and Purification, 130, pp.44-
837 54.
838 Kaufmann, T., Harrison, P., Richardson, M., Pinheiro, T. and Wall, M. (2016).
839 Intracellular soluble α-synuclein oligomers reduce pyramidal cell excitability. The Journal
840 of Physiology, 594(10), pp.2751-2772.
841 Kerr, M., Wall, M. and Richardson, M. (2013). Adenosine A1receptor activation mediates
842 the developmental shift at layer 5 pyramidal cell synapses and is a determinant of
843 mature synaptic strength. The Journal of Physiology, 591(13), pp.3371-3380.
844 Kumar, S., Tepper, K., Kaniyappan, S., Biernat, J., Wegmann, S., Mandelkow, E., Müller,
845 D. and Mandelkow, E. (2014). Stages and Conformations of the Tau Repeat Domain
846 during Aggregation and Its Effect on Neuronal Toxicity. *Journal of Biological Chemistry*,
847 289(29), pp.20318-20332.

Lasagna-Reeves, C., Castillo-Carranza, D., Sengupta, U., Guerrero-Munoz, M., Kiritoshi, T., Neugebauer, V., Jackson, G. and Kayed, R. (2012). Alzheimer brain-derived tau oligomers propagate pathology from endogenous tau. Scientific Reports, 2(1).

Lee, V., Goedert, M. and Trojanowski, J. (2001). Neurodegenerative Tauopathies. Annual Review of Neuroscience, 24(1), pp.1121-1159.

Markram, H., Lübke, J., Frotscher, M., Roth, A. and Sakmann, B. (1997). Physiology and anatomy os synaptic connections between thick tufted pyramidal neurones in the developing neocortex. J Physiol 500, 409-440.

McInnes, J., Wierda, K., Snellinx, A., Bounti, L., Wang, Y., Stancu, I., Apóstolo, N., Gevaert, K., Dewachter, I., Spires-Jones, T., De Strooper, B., De Wit, J., Zhou, L. and Verstreken, P. (2018). Synaptogyrin-3 Mediates Presynaptic Dysfunction Induced by Tau. Neuron, 97(4), pp.823-835.e8.

Michel, C., Kumar, S., Pinotsi, D., Tunnacliffe, A., St. George-Hyslop, P., Mandelkow, E., Mandelkow, E., Kaminski, C. and Kaminski Schierle, G. (2013). Extracellular Monomeric Tau Protein Is Sufficient to Initiate the Spread of Tau Protein Pathology. *Journal of Biological Chemistry*, 289(2), pp.956-967.

Mirbaha, H., Chen, D., Morazova, O., Ruff, K., Sharma, A., Liu, X., Goodarzi, M., Pappu, R., Colby, D., Mirzaei, H., Joachimiak, L. and Diamond, M. (2018). Inert and seed-competent tau monomers suggest structural origins of aggregation. *eLife*, 7.

Mondragón-Rodríguez, S., Salas-Gallardo, A., González-Pereyra, P., Macías, M., Ordaz, B., Peña-Ortega, F., … Williams, S. (2018). Phosphorylation of Tau protein correlates with changes in hippocampal theta oscillations and reduces hippocampal excitability in Alzheimer's model. The Journal of Biological Chemistry, 293(22), 8462–8472

Moreno H, Morfini G, Buitrago L, Ujlaki G, Choi S, Yu E, Moreira JE, Avila J, Brady ST, Pant H, Sugimori M, Llinás RR. (2016) Tau pathology-mediated presynaptic dysfunction. Neuroscience. 325:30-8.

874 Nelson PT, Break H, Markbery WR. Neuropathology and cognitive impairment in
875 Alzheimer disease: a complex but coherent relationship. J Neuropathol Exp Neural.
876 2009;68:1–14.
877 Ondrejcak, T., Klyubin, I., Corbett, G., Fraser, G., Hong, W., Mably, A., Gardener, M.,
878 Hammersley, J., Perkinton, M., Billinton, A., Walsh, D. and Rowan, M. (2018). Cellular
879 Prion Protein Mediates the Disruption of Hippocampal Synaptic Plasticity by Soluble Tau
880 In Vivo. The Journal of Neuroscience, 38(50), pp.10595-10606.
881 Puzzo, D., Piacentini, R., Fá, M., Gulisano, W., Li Puma, D., Staniszewski, A., Zhang, H.,
882 Tropea, M., Cocco, S., Palmeri, A., Fraser, P., D'Adamio, L., Grassi, C. and Arancio, O.
883 (2017). LTP and memory impairment caused by extracellular Aβ and Tau oligomers is
884 APP-dependent. eLife, 6.
885 Qiang, L., Sun, X., Austin, T., Muralidharan, H., Jean, D., Liu, M., Yu, W. and Baas, P.
886 (2018). Tau Does Not Stabilize Axonal Microtubules but Rather Enables Them to Have
887 Long Labile Domains. Current Biology, 28(13), pp.2181-2189.e4. Berger, Z., Roder, H.,
888 Hanna, A., Carlson, A., Rangachari, V., Yue, M., Wszolek, Z., Ashe, K., Knight, J.,
889 Dickson, D., Andorfer, C., Rosenberry, T., Lewis, J., Hutton, M. and Janus, C. (2007).
890 Accumulation of Pathological Tau Species and Memory Loss in a Conditional Model of
891 Tauopathy. Journal of Neuroscience, 27(14), pp.3650
892 Regan P, Piers T, Yi JH, Kim DH, Huh S, Park SJ, et al. Tau phosphorylation at serine
893 396 residue is required for hippocampal LTD. (2015) J Neurosci. 35:4804–4812.
894 Reyes, A. & Sakmann, B. (1999). Developmental switch in the short term modification of
895 unitary EPSPs evoked in layer 2/3 and layer 5 pyramidal neurons in rat neocortex. J
896 Neurosci 19, 3827-3835.
897 Richardson, M. J. E., & Silberberg, G. (2008). Measurement and Analysis of
898 Postsynaptic Potentials Using a Novel Voltage-Deconvolution Method. Journal of
899 Neurophysiology, 99(2), 1020–1031.

Rocher, A. B., Crimins, J. L., Amatrudo, J. M., Kinson, M. S., Todd-Brown, M. A., Lewis, J., & Luebke, J. I. (2010). Structural and functional changes in tau mutant mice neurons are not linked to the presence of NFTs. Experimental Neurology, 223(2), pp385–393.

Rudinskiy, N., Hawkes, J., Wegmann, S., Kuchibhotla, K., Muzikansky, A., Betensky, R., Spires-Jones, T. and Hyman, B. (2014). Tau pathology does not affect experience-driven single-neuron and network-wide Arc/Arg3.1 responses. Acta Neuropathologica Communications, 2(1).

Shammas, S., Garcia, G., Kumar, S., Kjaergaard, M., Horrocks, M., Shivji, N., Mandelkow, E., Knowles, T., Mandelkow, E. and Klenerman, D. (2015). A mechanistic model of tau amyloid aggregation based on direct observation of oligomers. Nature Communications, 6(1).

Spires, T., Orne, J., SantaCruz, K., Pitstick, R., Carlson, G., Ashe, K. and Hyman, B. (2006). Region-specific Dissociation of Neuronal Loss and Neurofibrillary Pathology in a Mouse Model of Tauopathy. The American Journal of Pathology, 168(5), pp.1598-1607.

Tamagnini, F., Walsh, D. A., Brown, J. T., Bondulich, M. K., Hanger, D. P., & Randall, A. D. (2017). Hippocampal neurophysiology is modified by a disease-associated C-terminal fragment of tau protein. Neurobiology of Aging, 60, pp44–56.

Tanemura, K., Murayama, M., Akagi, T., Hashikawa, T., Tominaga, T., Ichikawa, M., Yamaguchi, H. and Takashima, A. (2002). Neurodegeneration with Tau Accumulation in a Transgenic Mouse Expressing V337M Human Tau. The Journal of Neuroscience, 22(1), pp.133-141.

Tatebayashi, Y., Miyasaka, T., Chui, D., Akagi, T., Mishima, K., Iwasaki, K., Fujiwara, M., Tanemura, K., Murayama, M., Ishiguro, K., Planel, E., Sato, S., Hashikawa, T. and Takashima, A. (2002). Tau filament formation and associative memory deficit in aged mice expressing mutant (R406W) human tau. Proceedings of the National Academy of Sciences, 99(21), pp.13896-13901.

Teravskis, P., Covelo, A., Miller, E., Singh, B., Martell-Martínez, H., Benneyworth, M., Gallardo, C., Oxnard, B., Araque, A., Lee, M. and Liao, D. (2018). A53T Mutant Alpha-

928 Synuclein Induces Tau-Dependent Postsynaptic Impairment Independently of
929 Neurodegenerative Changes. The Journal of Neuroscience, 38(45), pp.9754-9767.
930 Tracy, T. and Gan, L. (2018). Tau-mediated synaptic and neuronal dysfunction in
931 neurodegenerative disease. Current Opinion in Neurobiology, 51, pp.134-138.
932 Uhlenbeck GE & Ornstein LS (1930). On the theory of the Brownian motion. Phys Rev
933 36, 823–841.
934 von Bergen, M., Barghorn, S., Biernat, J., Mandelkow, E.-M., Mandelkow, E., (2005).
935 Tau aggregation is driven by a transition from random coil to beta sheet structure.
936 Biochimica et Biophysica Acta (BBA) - Molecular Basis of Disease, The Biology and
937 Pathobiology of Tau 1739, 158–166.
938 Wittman, C.W., Wszolek, M. F., Shulman, J. M., Salvaterra, P. M., Lewis, J., Hutton, M.,
939 Feany, M.B., (2001) Tauopathy in Drosophila: Neurodegeneration without Neurofibrillary
940 Tangles. Science, 293(5530) pp.
941 Yoshiyama, Y., Higuchi, M., Zhang, B., Huang, S., Iwata, N., Saido, T., Maeda, J.,
942 Suhara, T., Trojanowski, J. and Lee, V. (2007). Synapse Loss and Microglial Activation
943 Precede Tangles in a P301S Tauopathy Mouse Model. Neuron, 53(3), pp.337-351.
944 Zhou, L., McInnes, J., Wierda, K., Holt, M., Herrmann, A. G., Jackson, R. J….
945 Verstreken, P. (2017). Tau association with synaptic vesicles causes presynaptic
946 dysfunction. Nature Communications, 8, pp15295
947
948
949
950
951
952
953
954
955

Legends

Fig. 1: Biochemical characterisation of recombinant tau-441oligomers.

(A) Schematic illustration of full length tau-441 showing the two N-terminus repeats (N1, N2) and the four microtubule-binding repeat domains (R1-R4). To ensure specific labelling with Alexa Fluor 488 C5-maleimide (AF maleimide) on a single cysteine outside the central core of the microtubule repeat region (R1-R4), the two native cysteine residues were each modified to alanine (C291A and C322A, shown as black dots below R2 and R3) and a new cysteine residue introduced at residue 260 (I260C) in R1. This approach has been shown not to have any major effects on the structure and function of tau (see Materials and Methods). (B) Representative negative-stain transmission electron-microscopy micrograph showing that maleimide-labelled oTau has a granular/spherical conformation. The insert shows a single structure at higher magnification. (C) Electron micrograph of negative control (buffer + label only) shows no granular structures. Scale bars = 200 nm and 20 nm for high-magnification insert. (D) Dot-blots illustrating the immunoreactivity of oTau that has been dissolved into intracellular recording solution: Lane 1, intracellular recording solution alone; lane 2, intracellular recording solution + oTau, which was filtered after the oTau was added; lane 3, intracellular recording solution filtered before addition of oTau. Filtration after addition of oTau decreased the presence of oTau as detected with three different antibodies. Thus in

the electrophysiology experiments the intracellular solution was filtered prior to oTau addition. (E) CD spectra for oTau showing a prominent negative peak at ~208 nm, indicating the presence of β sheets (F) Dynamic light scattering (DLS) distributions shows that monomeric Tau particles are small with a narrow size distribution (~80% particles measuring at 7.5 – 10nm). In contrast, oTau particles are larger and have a much wider size distribution (~93% of the particles at 18-32 nm).

Figure Contributions: EH and TKK performed the experiments and analysed the data

Figure 2. oTau localisation in injected neurons and extraction of electrophysiological parameters.

(A) Micrograph of a labelled hippocampal CA1 pyramidal cell (red) with oTau (green) present in the cell body. The tau protein is labelled with AF-488 maleimide and the neuron is filled with AF-594 dye. Scale bar 14 μm. (B) Illustration of the standard IV protocol used to extract neural parameters: current steps start from -200 to -300 pA and are increased by 50 pA (top panel) until a regular firing pattern is induced (bottom panel). Current steps around the resting potential were used to extract the input resistance. (C) The dynamic IV protocol injects a naturalistic current into the cell (top panel) and the voltage recorded (bottom panel) is used to extract a set of parameters using the dynamic IV method and to determine the firing rate. (D) Mean ionic current I_{ion} is plotted against membrane potential (grey). The black line is the dynamic IV curve generated by the average current at a particular voltage (in 1 mV bins). (E) The negative of I_{ion}/C is then plotted (grey) along with the EIF (exponential integrate-and-fire) computational model fit, black line. From this curve a number of subthreshold parameters can be extracted (such as resting potential E, time constant τ and spike-threshold voltage V_T). *Figure Contributions:* EH performed the experiments and analysed the data.

Figure 3. oTau induces little change in sub-threshold electrophysiological parameters until late time points

(A) The membrane-potential response to naturistic current injection (left panel) from a hippocampal CA1 pyramidal cell injected with vehicle at time zero (after whole-cell breakthrough, top) and after 40 minutes of recording (bottom). The inset shows parts of the membrane-potential response at an expanded time base illustrating that there is no significant change in the voltage response to naturalistic current injection over time. The standard current-voltage response (right panel) also does not change during recording. (B) The membrane-potential response to naturistic current injection (left panel) from a pyramidal cell injected with oTau (133 nM) at time zero (after whole-cell breakthrough, top) and after 40 minutes of recording (bottom). The inset shows parts of the membrane response at an expanded time base illustrating little change in the voltage response to naturalistic current over-time although the action potential amplitude is smaller. Right panel, the standard current-voltage responses at time zero and after 40 minutes. (C) The membrane-potential response to naturistic current injection (left panel) from a pyramidal cell injected with oTau (444 nM) at time zero (after whole cell breakthrough), after 30 and 40 minutes of recording. There was a depolarisation over the time period leading to an increased firing rate at 30 and 40 minutes. The inset shows parts of the voltage response at an expanded time base illustrating little change in the electrophysiogical properties at 30 minutes but clear changes at 40 minutes. Right panel, the standard current-voltage response at time zero and after 30 and 40 minutes. There are clear changes in the standard current-voltage response (a marked increase in input resistance) after 40 minutes of recording (right panels) but not after 30 minutes.

Figure Contributions: EH performed the experiments and analysed the data.

Figure 4: oTau significantly changes action potential dynamics

(A) Examples of action potential waveforms recorded at time zero (left panel) and after 40 minutes (right panel) from hippocampal CA1 pyramidal cells injected with either vehicle, BSA

or oTau (44,133 or 444 nM). (B) Summaries of the changes in action potential parameters (amplitude, duration, rate of rise and rate of decay) from recordings with neurons injected with either vehicle, BSA or oTau (44,133 or 444 nM). For each treatment there are two bars with associated data points (mean values from single recordings): The first bar and associated points are from time zero and the second bar and associated points are after 40 minutes of recording. Amplitude was significantly decreased in all three tested concentrations of tau between time points 0 and 40 mins (44 nM p=0.0641, 133 nM p=0.00054, 444 nM p=0.00228). Action potential width increased significantly in cells where 444 nM oTau was introduced (p=0.0156). The rate of rise and decay were also altered following introduction of oTau. Rise was significantly slower for all three concentrations of oTau (44 nM p=0.0641, 133 nM p=0.00054 and 444 nM p=0.002228). Whereas, decay was significantly slower only for 444 nM oTau, p=0.012. (C) Left panel shows the relative change in action potential amplitude plotted against time for cells injected with oTau (44,133 or 444 nM). Action potential amplitudes are normalised to the amplitude at time-zero. Right panel shows examples of average action potential waveforms recorded at different time points from neurons injected with either 133 or 444 nM oTau illustrating the change in amplitude. (D) Left panel shows the relative change in action- potential rise against time for neurons injected with oTau (44,133 or 444 nM). The speed of rise has been normalised to the speed of rise of action potentials recorded at time-zero. Right panel shows superimposed and normalised action potential waveforms illustrating the effects of oTau at 133 nM and 444 nM on the rate of action potential rise against recording time.

Figure Contributions: EH performed the experiments and analysed the data.

Figure 5. Monomeric tau protein does not change action potential dynamics and the accumulation of oTau in the pipette cannot account for the effects on action potential dynamics

(A) Gel showing dimeric tau protein (lane A) and tau protein converted to monomers (mTau, in lanes labelled (B) There is no significant difference between current-voltage responses

from a hippocampal CA1 neurons injected with 444 nM of mTau measured at time-zero and after 40 minutes of recording. (C) Top panel shows examples of action potential waveforms recorded at time zero and after 40 minutes of recording from a neuron injected with 444 nM mTau. The mTau does not change the amplitude or kinetics of the action potential waveform. (C) Bottom panel summarises data from 5 neurons, showing that action potential amplitude does not change over time when neurons are injected with 444 nM mTau. (D) The mean series resistance plotted against time for neurons injected with vehicle, BSA or oTau (44,133, or 444 nM). There was no significant difference in series resistance between treatments and the series resistance did not significantly increase during recordings. (E) Diagram illustrating the control re-patching protocol. Pyramidal-cell recordings were made (20 minutes) with vehicle present in the intracellular solution. The patch-electrode was carefully removed from the cell and then the cell was re-recorded from using a new patch-electrode also containing vehicle. 9F). There was no change in action potential amplitude during the initial recording (at 20 minutes, action potential amplitude was 102 ± 4 % of the amplitude at time zero) and after re-recording with a new electrode (108 ± 11 % of amplitude at time zero, n = 4 neurons). Thus the re-patching protocol itself does not induce changes in action potential amplitude. (G) Shows examples of average action potential waveforms from a single recording. (H) Diagram illustrating the test re-patching protocol. Pyramidal cell recordings were made (20 minutes) with oTau (444 nM) in the intracellular solution. The patch-electrode was then carefully removed from the cell and the cell was then re-recorded from using a patch-electrode containing intracellular solution with vehicle. (I) In cells injected with oTau (444 nM), action potential amplitude decreased during the initial recording period (at 20 minutes, action potential amplitude was 84 ± 3.1 % of the amplitude at time zero) and remained depressed following re-recording with a new patch-electrode containing vehicle (81 ± 5 % of amplitude at time zero, n = 3). (J) Shows examples of average action potential waveforms from a single re-patching experiment with 444 nM oTau. These control experiments strongly suggest that the aggregation of oTau in the electrode or in the area

around the initial whole-cell break- through does not account for the observed changes in action potential dynamics.

Figure Contributions: EH performed the experiments and analysed the data.

Figure 6. Protocols for testing the effect of oTau on synaptic transmission between thick-tufted layer V somatosensory neocortical neurons

(A) Standard IV relationships recorded from neocortical layer-V pyramidal cells using pipettes containing either vehicle (top panels) or oTau (666 nM, bottom panels). There was no significant change in the IV relationship over 40 minutes in cells injected with vehicle, whereas oTau reduced action potential amplitude and increased cell input resistance. (B) Micrograph of three layer-V pyramidal cells labelled with AF-488. Recordings were routinely made from 3 neighbouring pyramidal cells to increase the probability of finding synaptically connected cells. (C) Diagram of experimental protocol for synaptically connected pyramidal cells: (top panel) oTau was introduced into the presynaptic cell and vehicle was introduced into the postsynaptic cell; (bottom panel) for control recordings, vehicle was introduced into both pre and postsynaptic neurons. (D) A train of 5 action potentials (20 Hz) and 1 recovery action potential were evoked in the presynaptic cell with short depolarising current steps (top) and the resultant EPSPs were recorded in the postsynaptic cell (bottom). (E) Expanded traces of the first action potential (in the train) and the resultant EPSP illustrating the measurement of first EPSP amplitude and latency. (F) Method of accurately measuring the amplitude of the 2^{nd} to 5^{th} EPSPs in the train. EPSPs were averaged (after removing any baseline drift) and then deconvolved. The deconvolved EPSPs were cropped out and then reconvolved so that individual average EPSPs were not superimposed on the decay of the previous EPSP average. The accuracy of the deconvolution method was confirmed by reconvolving the EPSPs and comparing the resultant waveforms to the original untransformed EPSPs.

Figure Contributions: EH performed the experiments and analysed the data.

Figure 7: Presynaptic oTau impairs synaptic transmission between layer 5 pyramidal cells

(A) The amplitude of the first EPSP in the train (relative to the amplitude of averaged EPSPs over the first 10 minutes of the recording) plotted against time for synaptically connected pairs with either vehicle or oTau (666 nM) introduced into the presynaptic cell. There was little change in the amplitude of EPSPs for connections where vehicle was introduced into pre and postsynaptic cells (over 50 minutes) but there was a significant decline in the amplitude of EPSPs when oTau was introduced into the presynaptic cell (control vs tau 30-40 mins p=0.0293, 40-50 mins p=0.0344). (B) Example of averaged first EPSPs at different time points when either vehicle or oTau was introduced into the presynaptic cell. The EPSPs are averages of 30-50 sweeps and have been deconvolved, cropped and then reconvolved (as outlined in Figure 6). (C) Graph plotting the amplitude of average EPSPs (relative to the amplitude of the first EPSP) against number in the train for 0-10 minutes of recording and for 30-40 minutes of recording, where vehicle was introduced into both pre and postsynaptic cells. There was a small but significant increase in depression between time 0 and 30-40 mins for the 2^{nd} EPSP (p=0.0316) and the 5^{th} EPSP (p=0.0409) in the train. (D) Example EPSP waveforms from a single recording when vehicle was introduced into both the pre and postsynaptic cells. Averages were constructed at 0-10 minutes (left panel) and at 30-40 minutes (right panel) and are normalised so the amplitude of the first EPSP remains the same. There is little change in the degree of depression over time. (E) Graph plotting the average relative amplitude of EPSPs (relative to the first EPSP) against number in the train at 0-10 minutes and at 30-40 minutes with oTau present in the presynaptic cell. There was a significant increase in depression between 0 and 30-40 mins for the 2^{nd} EPSP 2 (p =0.0347), 3^{rd} EPSP (p=0.0365) and 4^{th} EPSP (p=0.00941) in the train. (F) Example EPSP waveforms from a single recording when oTau was introduced into the presynaptic cell. Averages were constructed at 0-10 minutes (left panel) and at 30-40 minutes (right panel) and are normalised so the amplitude of the first EPSP remains the same. The 3^{rd}-5^{th} EPSPs (arrows) are absent in the 30-40 minute average although the action potentials did not fail in the

presynaptic cell. (G) Graphs plotting paired pulse ratio (amplitude of second EPSP/ amplitude of first EPSP) for cells with vehicle present and for recordings when oTau was introduced into the presynaptic cell. The points are means from single experiments and the bars show the mean and SEMs for all recordings. In both treatments there was a significant fall in the paired-pulse ratio over the duration of the recording (vehicle p=0.0316 and oTau p=0.0347). (H) Graph plotting the percentage recovery in EPSP amplitude measured by evoking an EPSP 1 s after the end of the train. If there ws 100 % recovery then the recovery EPSP has the same amplitude as the first EPSP. The amount of recovery decreases over time and is similar for cells with either vehicle or oTau introduction. Right panel, waveforms after 30-40 minutes (same recording as in F) showing the absence of the 3rd-5th EPSPs, but there is some recovery in transmission after a 1s interval (inset shows mean recovery EPSP).

Figure Contributions: EH performed the experiments and analysed the data.

Figure 8. Introduction of oTau into postsynaptic neurons has no significant effect on basal synaptic transmission

(A) Diagram of experimental protocol: vehicle was introduced into the presynaptic cell and oTau (666 nM) was introduced into the postsynaptic cell. (B) The amplitude of the first EPSP in the train (relative to the amplitude of averaged EPSPs over the first 10 minutes of the recording) plotted against time with oTau present in the postsynaptic cell. There was no significant change in the amplitude of the first EPSP amplitude in the train for the duration of recordings. (C) Examples of averaged EPSPs (first in train) at different time points throughout the recording (oTau present in the postsynaptic cell). The EPSP averages have been deconvolved, cropped and then reconvolved (as in Figure 6). (D) The mean amplitude of the 2nd-5th EPSPs in the train normalised to the amplitude of the first EPSP in the train, averaged at 0-10 minutes and at 30-40 minutes. There was no significant change in the

1176 degree of short term depression over that time period. (E) Average EPSP waveforms from a
1177 single recording where oTau was introduced into the postsynaptic cell. Averages were
1178 constructed at 0-10 minutes (left panel) and at 30-40 minutes (right panel) and are not
1179 normalised.
1180 *Figure Contributions:* EH performed the experiments and analysed the data.
1181
1182 **Figure 9. Introduction of oTau into the postsynaptic neuron blocks the induction of**
1183 **LTP**
1184 (A) Diagram of experimental methods to measure long-term potentiation (LTP). EPSPs were
1185 recorded in CA1 hippocampal pyramidal cells in response to Schaffer collateral stimulation.
1186 LTP was induced by theta burst stimulation (TBS). (B) Mean EPSP amplitude plotted against
1187 time for 7 slices in control (vehicle introduced into pyramidal cells) and in 3 slices where the
1188 NMDA receptor antagonist L689,560 (5 μM) was present. TBS evoked robust potentiation in
1189 control conditions which was abolished by L689,560. Inset, average waveforms before (1)
1190 and 30 minutes after TBS (2) in control conditions and in the presence of L689,560 (5 μM).
1191 (C) Mean EPSP amplitude plotted against time for 7 slices with oTau (444 nM) present in the
1192 intracellular recording solution. LTP was abolished. Inset, average waveforms before (1) and
1193 30 minutes after TBS (2). (D) Mean EPSP amplitude against time for 5 slices with oTau (44
1194 nM) present in the intracellular recording solution. LTP was abolished but there is some
1195 short term potentiation. Inset, average waveforms before (1) and 30 minutes after TBS (2).
1196 (E) Graph plotting mean EPSP amplitude against time for 5 slices with monomeric Tau (444
1197 nM) present in the intracellular recording solution. LTP was induced in the presence of
1198 monomeric Tau. Inset, average waveforms before (1) and 30 minutes after TBS (2). (F)
1199 Summary. In control conditions (vehicle in the intracellular solution) after 30 minutes
1200 following TBS, EPSP amplitude was potentiated to 3.31 ± 1.32X baseline amplitude (n = 7).
1201 This potentiation was lost in the presence of L689,560 (0.53 ± 0.14, n = 3), with oTau 444
1202 nM in the intracellular solution (0.989 ± 0.31, p=0.042, n = 7, control vs 444 nM) and with 44

nM oTau in the intracellular solution (1.11 ± 0.1, *n* = 5). In contrast potentiation persisted with mTau (444 nM) in the intracellular solution (3.35 ± 0.90, *n* = 5). One-way ANOVA gives a significant effect of treatment (F(4,22)=5.645, p=0.0028) and Fisher posthoc comparisons shows significant differences between the potentiation of cells injected with vehicle and L689,560, 44 nM or 444 nM oTau (p=0.0055, p=0.0077 and p=0.0018 respectively). (G) Example voltage responses to the first burst in the TBS for a neuron where vehicle was introduced, where 444 nM oTau was introduced and where 44 nM oTau was introduced. (H) Photomicrographs of the dendrite bifurcation from a labelled hippocampal neuron where 444 nM of oTau was introduced at the soma. Left panel, dendrites labelled with AlexaFluor 594 introduced from patch pipette. Middle panel, fluorescent puncta of oTau. Right Panel, merged image showing dendrites (red) and oTau puncta (green). Scale bar 12 μM.

Figure Contributions: EH performed the experiments and analysed the data.

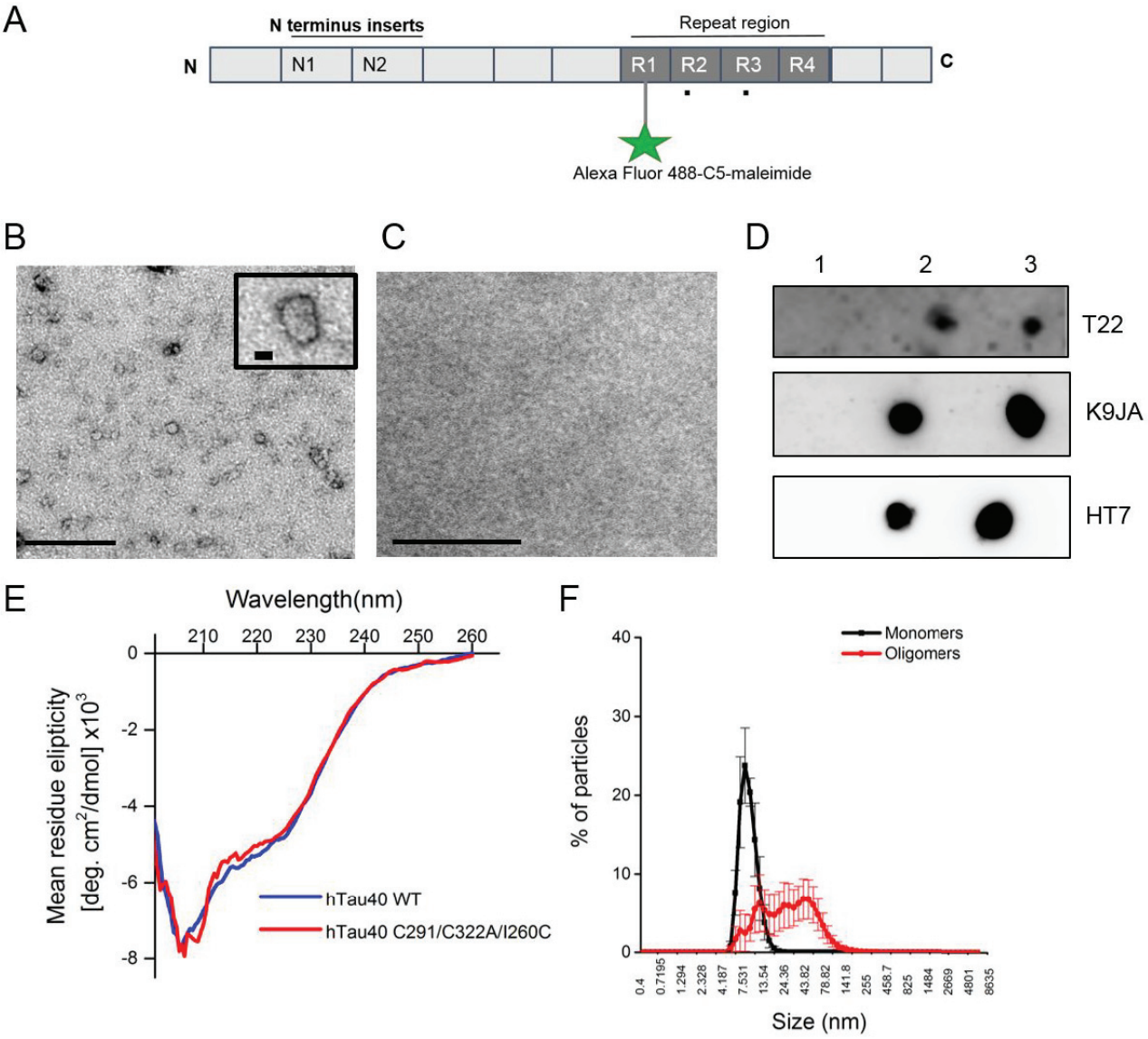

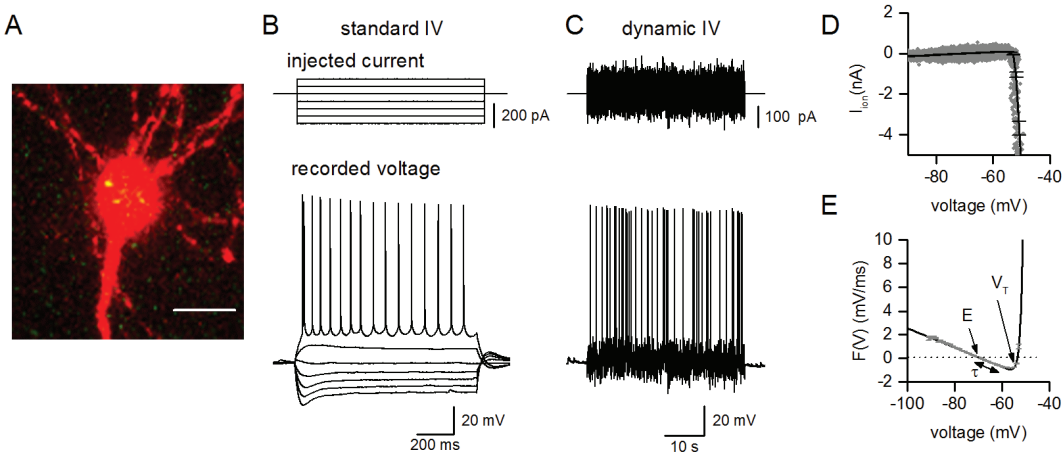

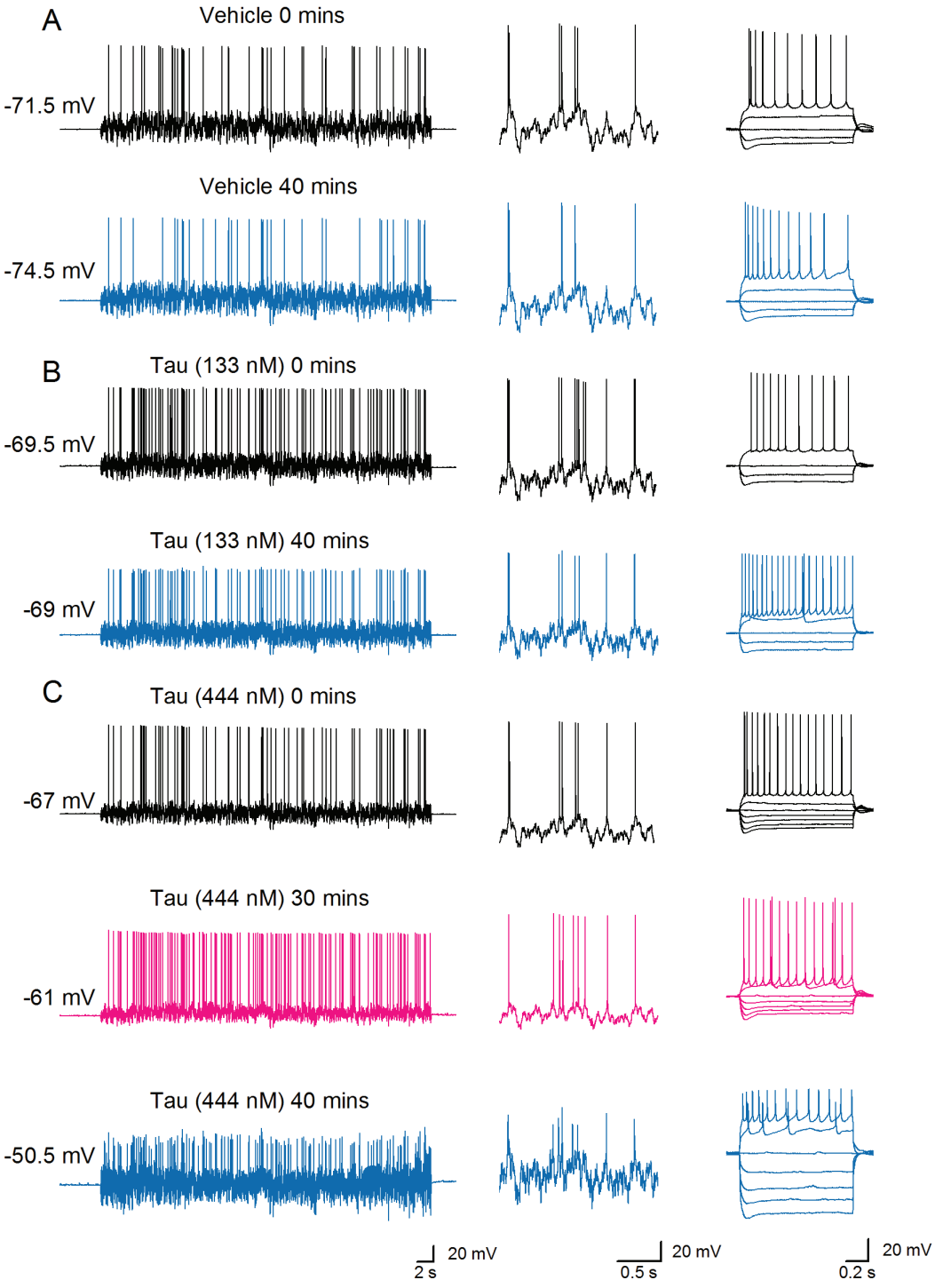

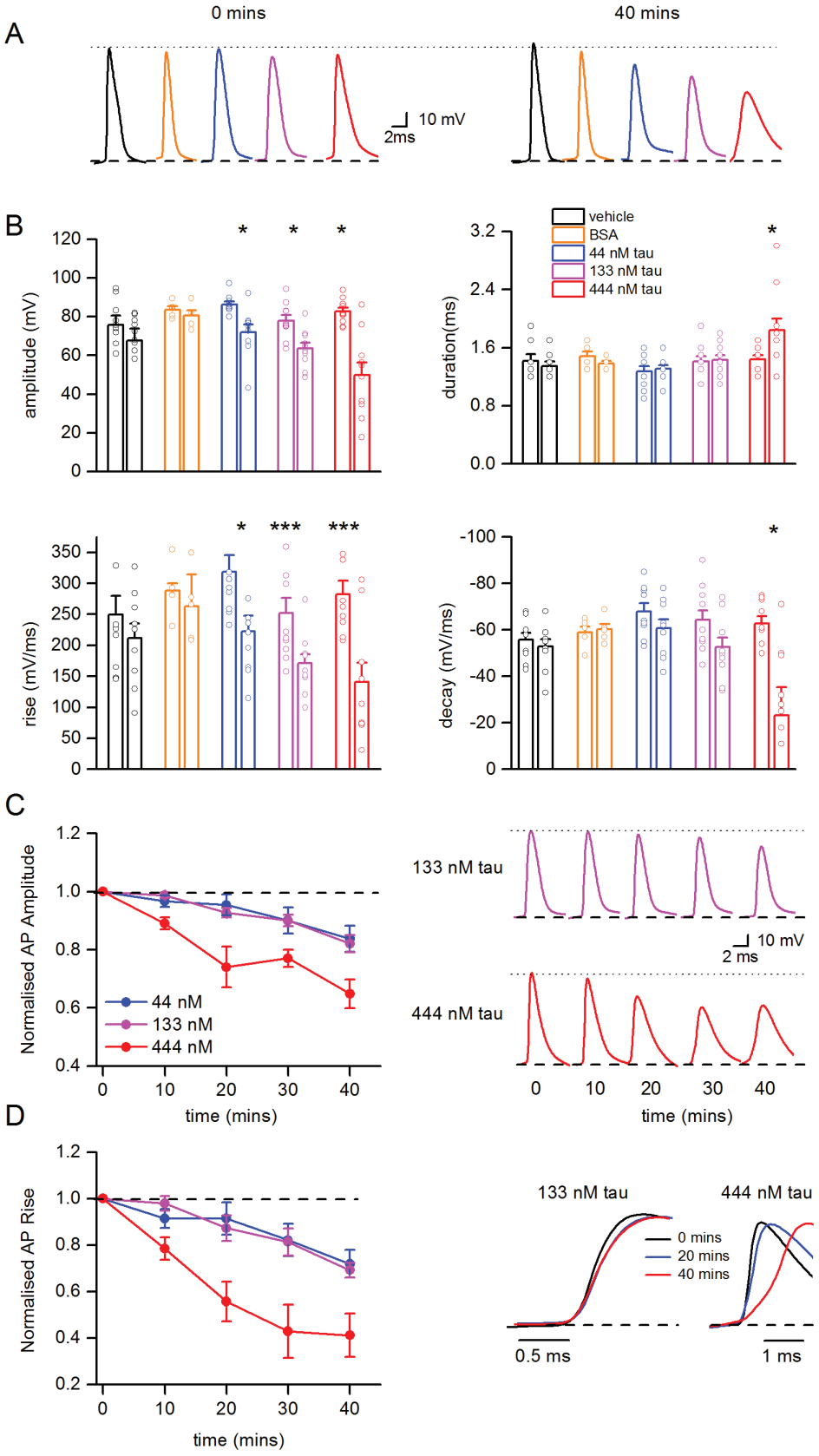

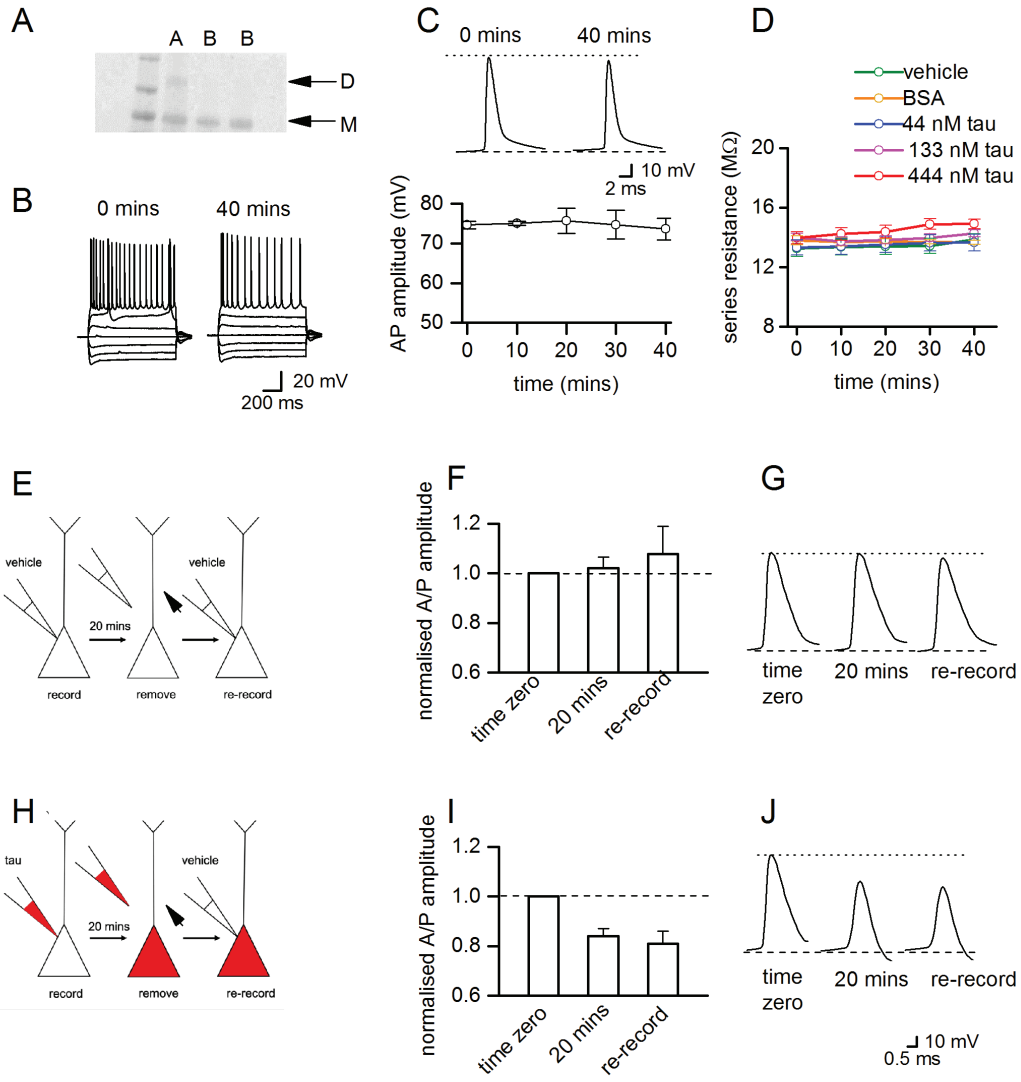

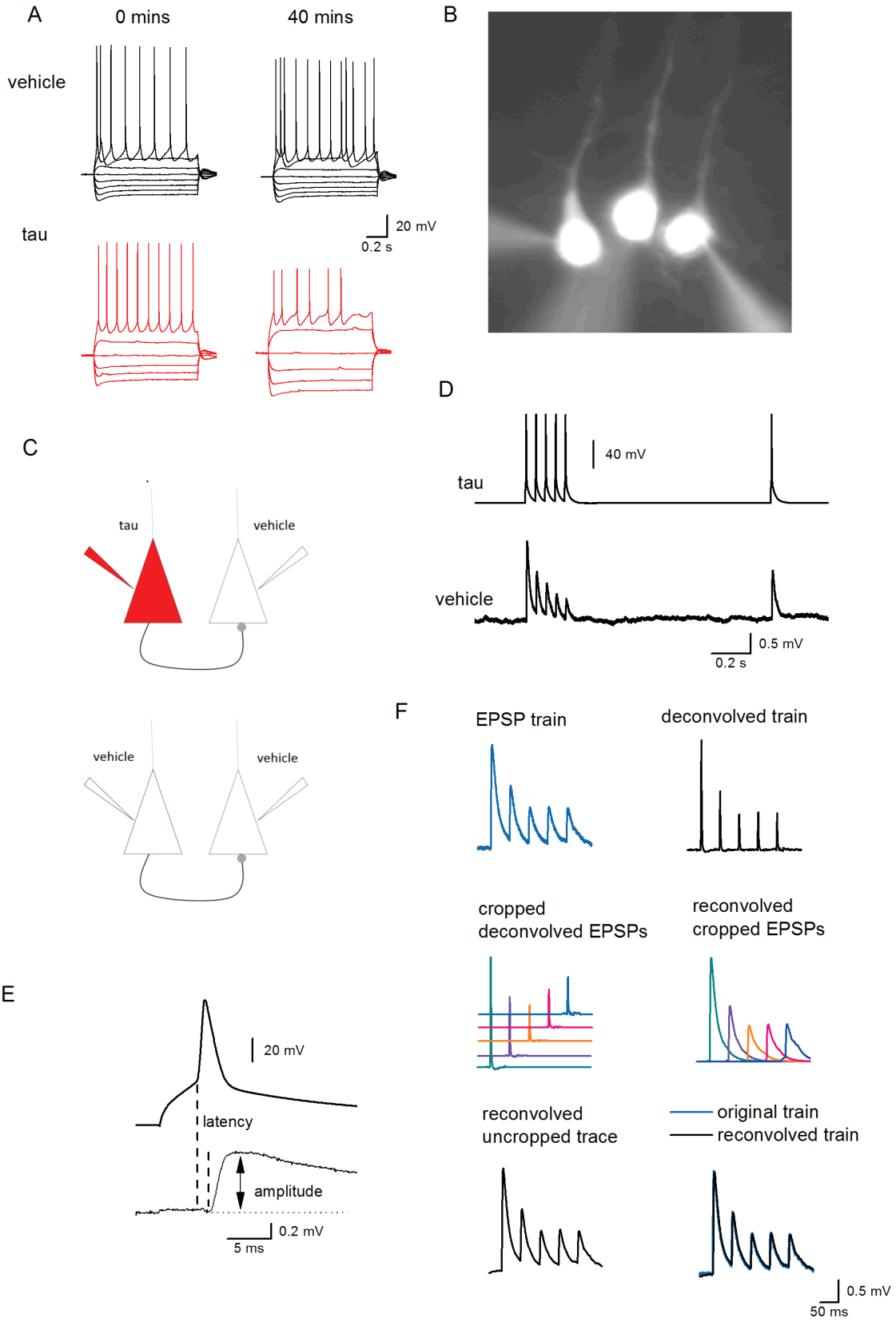

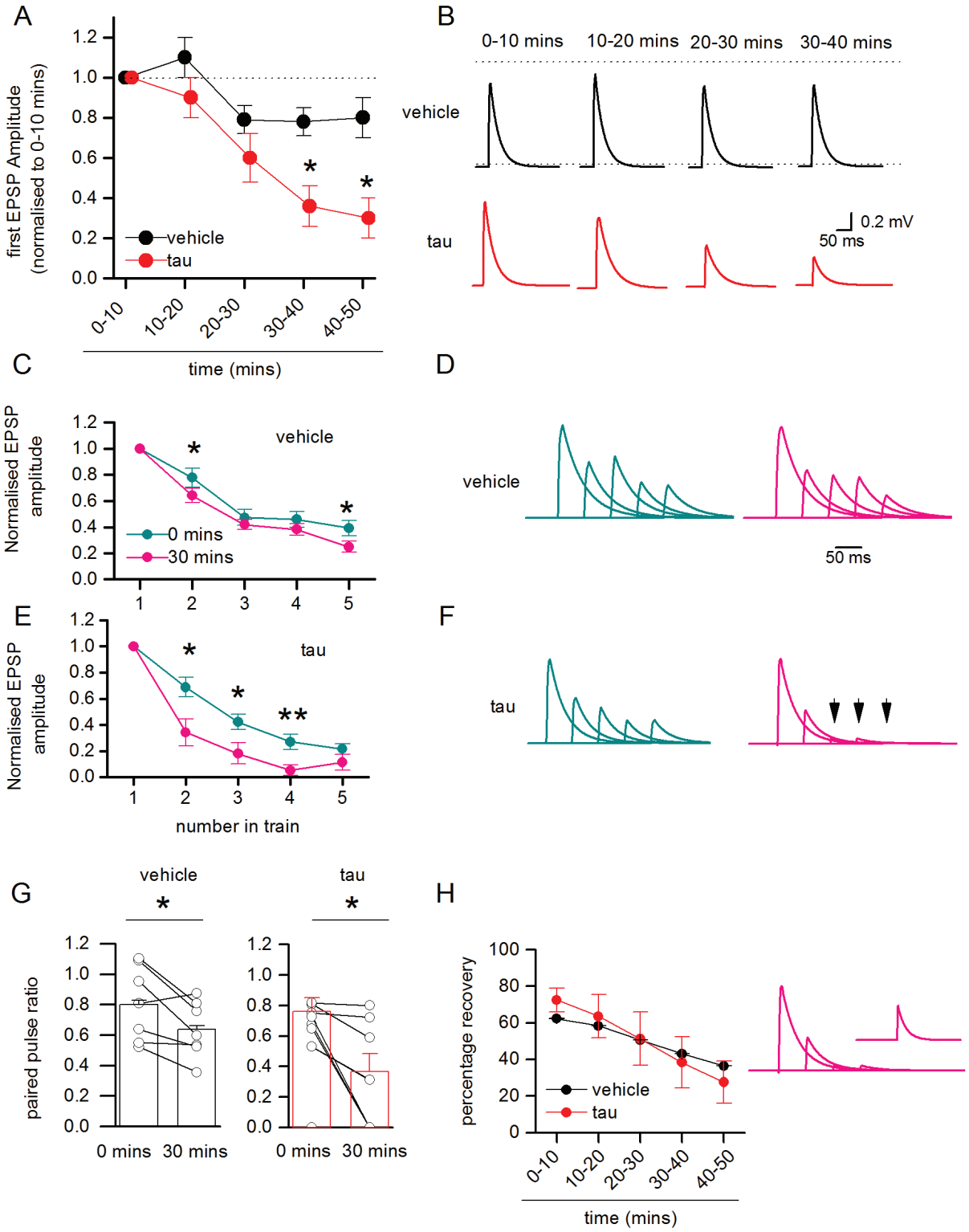

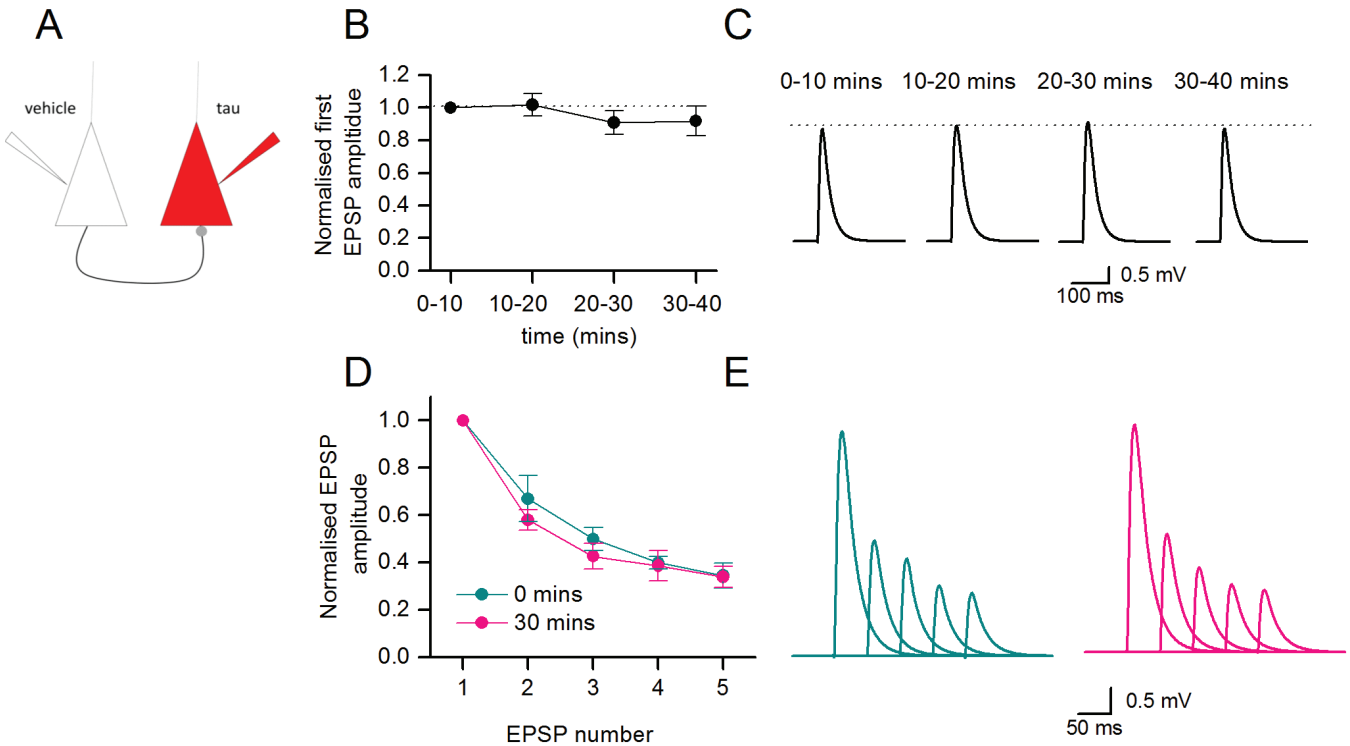

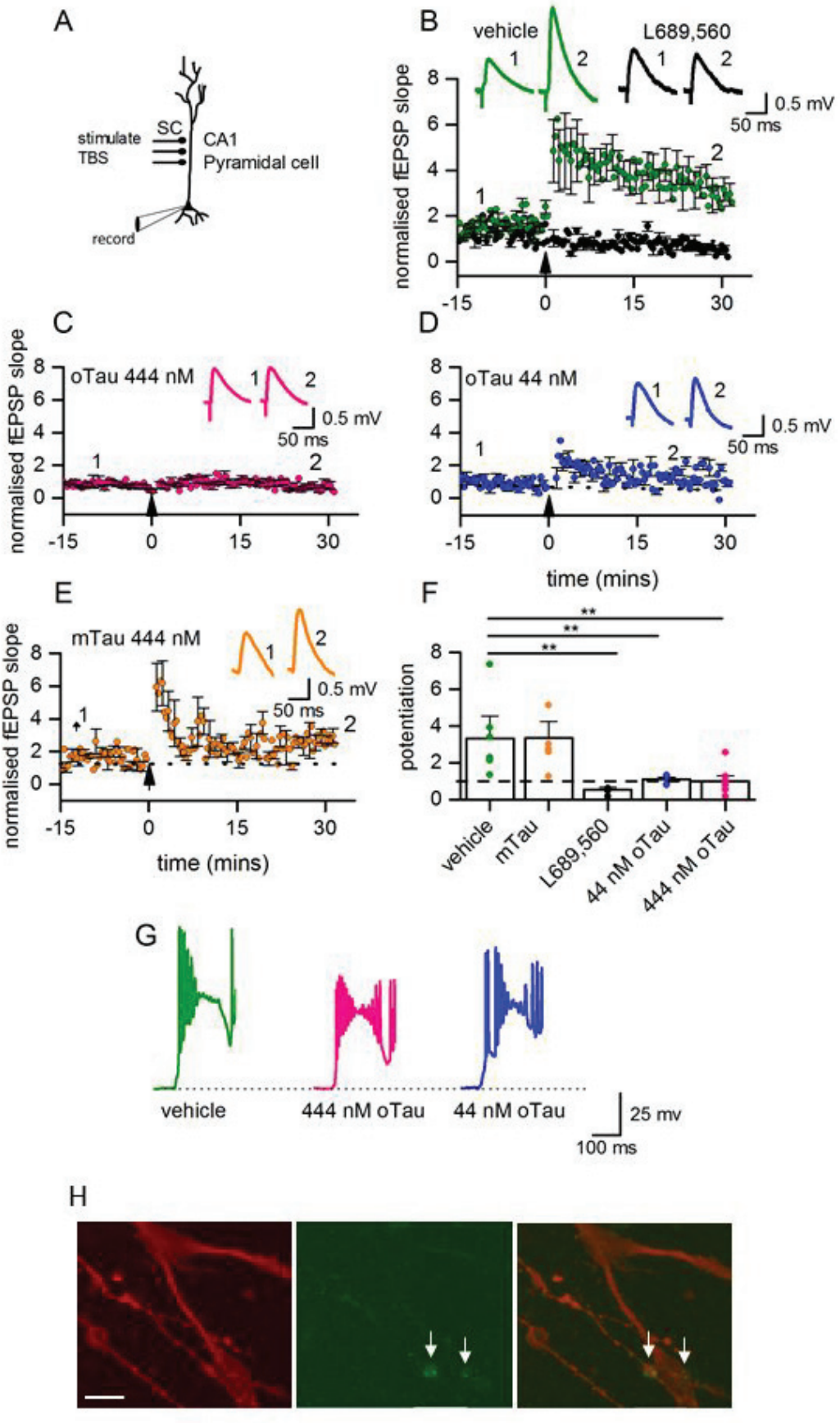

Table 1

	Vehicle			BSA			44 nM oTau			133 nM oTau			444 nM oTau		
Parameter	Mean	SEM	SD	Mean	SEM	SD	Mean	SEM	SD	Mean	SEM	SD	Mean	SEM	SD
C (pF)	121.8	± 12.56	± 62.8	125.6	± 14.17	± 34.43	132.55	± 17.65	± 79.43	105	± 8.04	± 44.22	125.3	± 14.31	± 71.55
R in (MΩ)	164.4	± 12.22	± 61.1	183.6	± 21.13	± 52.83	157.89	± 23.01	± 103.55	180.36	± 20.42	± 112.31	176.8	± 4.74	± 23.7
τ (ms)	20.72	± 1.75	± 8.75	15.72	± 0.89	± 2.23	16.67	± 1.86	± 8.37	15.24	± 1.40	± 7.7	19.63	± 2.25	± 1.25
E (mV)	-67.2	± 1.16	± 5.8	-68.5	± 1.34	± 3.35	-69.63	± 0.91	± 4.10	-66.22	± 1.06	± 5.83	-64.95	± 2.0	± 10
V T (mV)	-50.07	± 0.68	± 3.4	-52.69	± 1.26	± 3.15	-54.8	± 0.984	± 4.43	-50.67	± 1.35	± 7.43	-50.92	± 1.49	± 7.45
ΔT (mV)	0.77	± 0.036	± 0.18	0.82	± 0.063	± 0.16	0.97	± 0.15	± 0.68	0.87	± 0.1	± 0.55	0.89	± 0.08	± 0.4
Action potential															
amplitude (mV)	75.8	± 4.87	± 24.35	83.6	± 1.84	± 4.6	86.11	± 1.59	± 7.16	77.91	± 2.82	± 15.51	82.66	± 1.9	± 9.5
duration (ms)	1.42	± 0.093	± 0.465	1.48	± 0.07	± 0.18	1.28	± 1.31	± 5.90	1.41	± 0.07	± 0.385	1.44	± 0.053	± 0.265
rise(mV/ms)	249.4	± 30.54	± 152.7	288.4	± 17.8	± 44.5	318.8	± 26.55	± 119.48	252.7	± 23.68	± 130.24	282.11	± 21.85	± 109.25

Table 1: Electrophysiological parameters measured for CA1 hippocampal pyramidal cells at time zero for all experimental treatments.

See extended data table 1-1 for the mean, standard error of the mean (SEM) and standard deviation (SD) for all other recorded parameters.